

Detection of Intermittent Faults Based on an Optimally Weighted Moving Average T^2 Control Chart with Stationary Observations

Yinghong Zhao^{a,c}, Xiao He^a, Junfeng Zhang^a, Hongquan Ji^b, Donghua Zhou^{b,a,*}, Michael G. Pecht^c

^aDepartment of Automation, Beijing National Research Center for Information Science and Technology (BNRist), Tsinghua University, Beijing 100084, China

^bCollege of Electrical Engineering and Automation, Shandong University of Science and Technology, Qingdao 266590, China

^cCenter for Advanced Life Cycle Engineering (CALCE), University of Maryland, College Park, MD 20742, USA

Abstract

The moving average (MA)-type scheme, also known as the smoothing method, has been well established within the multivariate statistical process monitoring (MSPM) framework since the 1990s. However, its theoretical basis is still limited to smoothing independent data, and the optimality of its equally or exponentially weighted scheme remains unproven. This paper aims to weaken the independence assumption in the existing MA method, and then extend it to a broader area of dealing with autocorrelated weakly stationary processes. With the discovery of the non-optimality of the equally and exponentially weighted schemes used for fault detection when data have autocorrelation, the essence that they do not effectively utilize the correlation information of samples is revealed, giving birth to an optimally weighted moving average (OWMA) theory. The OWMA method is combined with the Hotelling's T^2 statistic to form an OWMA T^2 control chart (OWMA-TCC), in order to detect a more challenging type of fault, i.e., intermittent fault (IF). Different from the MA scheme that puts an equal weight on samples within a time window, OWMA-TCC uses correlation (autocorrelation and cross-correlation) information to find an optimal weight vector (OWV) for the purpose of IF detection (IFD). In order to achieve a best IFD performance, the concept of IF detectability is defined and corresponding detectability conditions are provided, which further serve as selection criteria of the OWV. Then, the OWV is given in the form of a solution to nonlinear equations, whose existence is proven with the aid of the Brouwer fixed-point theory. Moreover, symmetrical structure of the OWV is revealed, and the optimality of the MA scheme for any IF directions when data exhibit no autocorrelation is proven. Finally, simulations on a numerical example and the continuous stirred tank reactor process are carried out to give a comprehensive comparison among OWMA-TCC and several existing static and dynamic MSPM methods. The results show a superior IFD performance of the developed methods.

Keywords: Weighted moving average, optimal weight, intermittent faults, fault detection and detectability

1. Introduction

Fault detection (FD) for industrial processes with multivariate statistical process monitoring (MSPM)

methods has been a hot topic in the past few decades [1–3]. MSPM methods use various control charts to check statistical properties of process variables, among which T^2 control chart is one of the most effective ones since the Hotelling's T^2 statistic is admissible and most powerful in certain classes of hypothesis tests [4]. Permanent faults (PFs) are serious threats to the system reliability, since once PFs occur, they take effect permanently unless removed by external intervention. In practice, many kinds of PFs evolve gradually from intermittent faults (IFs) [5]. This implies that if faults are detected in this early stage, severe damage caused by PFs, such as system disruptions, plant shutdowns and even safety accidents, can be effectively avoided. In this

*This work was supported by the National Natural Science Foundation of China (NSFC) under Grants 61751307, 61733009, the Research Fund for the Taishan Scholar Project of Shandong Province of China (LZB2015-162), and the Key Project from Natural Sciences Foundation of Guangdong Province under Grant 2018B030311054. Corresponding author: Donghua Zhou.

Email addresses: zyh14@mails.tsinghua.edu.cn (Yinghong Zhao), hexiao@mail.tsinghua.edu.cn (Xiao He), jf-zhang13@mails.tsinghua.edu.cn (Junfeng Zhang), jihongquansd@126.com (Hongquan Ji), zdh@mail.tsinghua.edu.cn (Donghua Zhou), pecht@umd.edu (Michael G. Pecht)

regard, the detection of IFs is an important means to improve the system reliability. IFs have been recently of noticeable interest, and thus a review of their current research status has been published [5].

The IF is a kind of non-permanent fault that lasts a limited period of time and then disappears without any treatment [5]. So far, the IF detection (IFD) problem has been investigated under both model-based [6, 7] and data-driven frameworks. As for data-driven methods, several powerful tools such as the signal analysis [8], decision forest [9], dynamic Bayesian network [10] and MSPM [11] methods have been utilized to detect IFs in different application domains. Signal analysis methods are suitable to process unidimensional signals that possess periodicity. Decision forest and dynamic Bayesian network methods can take full use of the historical data of various faults. MSPM methods are easy to handle high-dimensional and correlated variables, and historical fault data are not necessary.

Among various MSPM methods [11–21], principal component analysis (PCA) and canonical correlation analysis (CCA) were used for detecting intermittent sensor faults caused by electrical interference in a smart home sensor network [11]. The Gaussian Process (GP) method, which is a Bayesian non-parametric supervised learning approach, has been recently in widespread use for many regression and classification tasks. In [12], a GP regression (GPR) model was established to estimate the mean and variance of the occurring intermittent stochastic faults with available measurements, and to detect the IFs based on a minimum distance criterion. Moreover, the use of a least absolute selection and shrinkage operator (Lasso)-based variable selection algorithm in combination with the GPR model was presented for IFD [13]. In [14], PCA was utilized to detect IFs such as poor contact faults in multi-axle speed sensors of high-speed trains. Note that in these methods, no time window was employed.

In [15, 16], the T^2 statistic and a generic quadratic-form statistic, combined with the moving average (MA) method, were utilized to detect IFs under the independent and multivariate Gaussian distribution assumption. In [17], dynamic PCA (DPCA) was applied to the measurement data of a gyroscope in order to detect its IFs. An exponentially weighted MA (EWMA)-based adaptive thresholding scheme was developed in [18] to detect IFs through T^2 and Q statistics resulting from PCA. The adaptive threshold was updated by a modified EWMA control chart with limited window length, and was effective in reducing the fault clearance time delay between the real disappearance of IFs and the recovery of the fault indicator. The developed adaptive thresh-

olding scheme was successfully applied to the detection of IFs in a cement rotary kiln [19]. In [20], a nonparametric Kullback-Leibler (KL) divergence resulting from multiblock PCA and moving window (MW)-based kernel density estimation (KDE) was presented to detect intermittent voltage sags in rooftop mounted PV (RMPV) systems. In [21], the Kantorovich distance (KD), a metric originates from the optimal transport theory, between two sets of time series data (one of which employed an MW to update the online samples) was employed to detect IFs.

In practice, many IFs have small magnitudes and short durations [5], which make them even more difficult to detect than incipient faults. Moreover, system dynamics and multi-level closed-loop control make industrial data autocorrelated. Due to the high-speed sampling requirement for capturing IFs, the property of non-independence in data is stronger and thus non-ignorable during IFD. As a result, existing MSPM methods have the following problems that limit their application to IFD. On the one hand, static MSPM methods, which use only a single observation for FD such as the PCA-based control chart, have been found [22–24] inefficient for small shifts, let alone IFs. Moreover, they cannot utilize autocorrelations in data. On the other hand, dynamic MSPM methods such as DPCA and canonical variate analysis (CVA) consider a time sequence of measurements and can capture process dynamics (i.e., utilize autocorrelations). However, time lags are chosen only according to system orders, but not considering the characteristics of IFs (i.e., the fault duration and magnitude). Therefore, they may not gain enough sensitivity to IFs, and their efficiency of detecting intermittent small shifts still needs further study.

The MA-type scheme is a simple and powerful smoothing tool that can enhance the statistics' sensitivity to faults in practical applications, and is easy to integrate with many MSPM and machine learning methods. Two related schemes are the equally and exponentially weighted schemes. When samples are independent and identically distributed, the covariance matrices of the averaged sample after MA and EWMA are $1/W$ and $\lambda/(2-\lambda)$ of the covariance matrix of the original sample respectively [25, 26], where W is the window length of MA and $0 < \lambda \leq 1$ is the weighting factor of EWMA. This overall reduction of the covariance brings about the smoothing effects of MA-type schemes, and consequently improves the FD performance. However, this theoretical basis holds only for independent data, and the statistical basis for the use of MA-type schemes to smooth autocorrelated data is still lost. In addition, both the MA and EWMA schemes

have a fixed weighted form. So far, the weighted MA (WMA) scheme that allows putting different weights on samples within a time window for the purpose of FD has not been fully investigated. Moreover, the optimality of these weighted schemes in terms of fault detectability remains unproven. These issues constitute the main motivations of our study.

This paper investigates the IFD problem in weakly stationary processes. A time window and a weight vector are employed to increase the sensitivity to IFs, and the window length is selected considering the characteristics of IFs. Main contributions of the paper are summarized as follows: 1) An optimally weighted moving average T^2 control chart (OWMA-TCC) with stationary observations is proposed. Different from existing methods that put an equal weight on samples within a time window, OWMA-TCC uses correlation (autocorrelation and cross-correlation) information to find an optimal weight vector. 2) The concept of IF detectability is defined and corresponding detectability conditions are provided, which further serve as selection criteria of the optimal weight. 3) The optimal weight is given in the form of a solution to nonlinear equations, whose existence is proven with the help of the Brouwer fixed-point theory. Moreover, the uniqueness of the optimal weight is proven in several special cases. 4) We reveal that the optimal weight possesses a symmetrical structure, and the MA scheme is optimal for any IF directions when data are independent, which gives more explanations for the rationality of existing MA-based methods. 5) Comprehensive comparative studies with existing static and dynamic MSPM methods, such as PCA, MA-PCA, DPCA, CVA and MW-KD, are carried out on a numerical example and the benchmark continuous stirred tank reactor (CSTR) process, which illustrate the superior IFD performance of the OWMA-TCC.

The remainder of this paper is organized as follows. In Section 2, the WMA-TCC with stationary Gaussian observations is introduced for the IFD problem. Then, the detectability of IFs by the WMA-TCC is analyzed in Section 3. The detectability conditions are further utilized to determine the optimal weight in Section 4. Section 5 extends these results to weakly stationary processes without the Gaussianity assumption. Simulation results are presented in Section 6, and conclusions are given in Section 7.

Notation: Except where otherwise stated, the notations used throughout the paper are standard. $\mathbb{N}_p(\mu, \Sigma)$ represents a p -dimensional normal distribution with expectation μ and covariance matrix Σ . $\mathbb{W}_p(N, \Sigma)$ represents a p -dimensional Wishart distribution with N degrees of freedom. $\mathbb{F}(p, N - p)$ is a central F distribution

with p and $N - p$ degrees of freedom. $\mathbb{F}_\alpha(p, N - p)$ is the $1 - \alpha$ percentile of the central F distribution with p and $N - p$ degrees of freedom. $\mathbb{G}\mathbb{P}_p(\mu, R_l)$ represents a p -dimensional stationary Gaussian process with expectation μ and autocovariance function matrix R_l . \mathbb{R}^n and $\mathbb{R}^{n \times m}$ denote the n -dimensional Euclidean space and the set of all $n \times m$ real matrices. $\|\xi\|$ and $\|\xi\|_\infty$ denote the Euclidean norm and infinity norm of a vector ξ , respectively. A^T , A^{-1} , $|A|$, $\text{tr}(A)$ and $\text{adj}(A)$ stand for the transpose, the inverse, the determinant, the trace and the adjoint of a matrix A , respectively. $\nabla_{\vec{a}_W} \mathcal{L}(\vec{a}_W, \lambda)$ is the gradient of \mathcal{L} with respect to \vec{a}_W . $\nabla_{\vec{a}_W}^2 \mathcal{L}(\vec{a}_W, \lambda)$ is the Hessian matrix of \mathcal{L} with respect to \vec{a}_W . Scalars $a_1 \cdots a_W$ form a row vector by $[a_1, a_2, \dots, a_W]$, and form a column vector by $[a_1; a_2; \dots; a_W]$. \triangleq is to give definition. $H_{l,l'}$ or $[H]_{l,l'}$ is an element of matrix H located in the l th row and l' th column. $H_{l,:}$ and $H_{:,l}$ are the l th row and l th column of matrix H , respectively. $\mathcal{T}_{\setminus j}$ is the matrix obtained from \mathcal{T} by deleting the row and column containing $\mathcal{T}_{i,j}$. I_p and e_{pi} denote the p -dimensional identity matrix and its i th column, respectively; 1_W and 0_W denote the W -dimensional column vectors with all of its entries being one and zero, respectively. The symbol \otimes denotes the Kronecker product and δ_{ij} is the Kronecker function. $\lambda_{\min}(\Gamma)$ and $\lambda_{\max}(\Gamma)$ are the minimum and maximum eigenvalues of matrix Γ , respectively. $A < B$ and $A \leq B$ mean that $A - B$ is negative definite and negative semidefinite, respectively.

2. Methodology

When the process is under steady-state operation and no operators change the process dynamics, the acquired data tends to be stationary, non-anomalous, and with no trends [18, 19]. Thus, the dynamics of practical in-control systems can be approximated by a stationary stochastic process. In this section, the WMA-TCC with stationary Gaussian observations is proposed for the purpose of FD in stationary Gaussian processes. The WMA-TCC in weakly stationary processes without the Gaussianity assumption is given in Section 5.

2.1. Preliminaries

The following lemma is the key result regarding Hotelling's T^2 distribution, see [27].

Lemma 1. *Let $T^2 = X^T S^{-1} X$, where X and S are independently distributed random variables with $X \sim \mathbb{N}_p(\mu, \Sigma)$ and $NS \sim \mathbb{W}_p(N, \Sigma)$, where $N \geq p$. Then*

$$T^2 \sim \frac{Np}{N - p + 1} \mathbb{F}(p, N - p + 1; \epsilon^2), \quad (1)$$

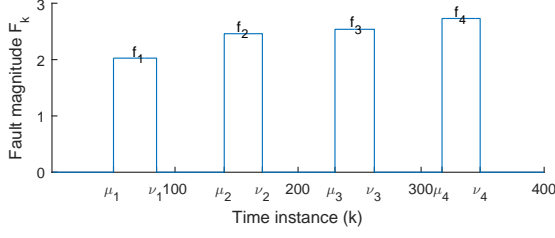


Figure 1: An example of intermittent faults.

imized. Thus, in this section, we analyze the IF detectability.

3.1. Guaranteed detectability

Consider the following widely used fault model in the MSPM framework [29–32]:

$$X_k^f = X_k^* + \Xi_k F_k, \quad (8)$$

where Ξ_k represents the fault direction, $\|F_k\|$ represents the fault magnitude, and X_k^* represents the process fluctuation under normal conditions, all in time instance k . Note that the above fault model can represent a multiple fault when the rank of the column vector F_k is larger than one. By introducing the time window, we have

$$\tilde{X}_k^f = \tilde{X}_k^* + \tilde{\Xi}_k \tilde{F}_k, \quad \tilde{X}_k^* = \sum_{j=1}^W a_j X_{k-j+1}^*, \quad (9)$$

where $\tilde{\Xi}_k \tilde{F}_k$ is the effect of all faults in the time window, and $\tilde{X}_k^* \sim \mathbb{N}_p(\mu, \tilde{\Sigma}_W)$. When we analyze the fault detectability, the following condition is introduced:

$$\|\tilde{S}_W^{-1/2}(\tilde{X}_k^* - \tilde{X})\|^2 \leq \delta^2. \quad (10)$$

Remark 1. Inequality (10) is commonly employed by literature addressing fault detectability problems in the MSPM framework [2, 26, 30, 33]. The condition means that the fault-free process \tilde{X}_k^* fluctuates within its acceptance region (7). Since a small significance level (i.e., $\alpha = 0.01$) is always selected, this condition holds with high probability. Note that this condition is only introduced to analyze detectability, and thus has no limitation to the practical application of the method.

Since $\Xi_k F_k \in \mathbb{R}^p$, it can be denoted by a scalar and a column vector whose norm is one. Then, in the case of IFs, as shown in Fig. 1, the corresponding fault model

can be represented [5, 34, 35] by

$$\Xi_k F_k = \sum_{q=1}^{\infty} [\Gamma(k - \mu_q) - \Gamma(k - \nu_q)] \xi_q f_q, \quad (11)$$

where $\Gamma(\cdot)$ is the step function; μ_q, ν_q represent the appearing and disappearing time of the q th IF, satisfying $\mu_q < \nu_q < \mu_{q+1}$; and $\xi_q \in \mathbb{R}^p, f_q \in \mathbb{R}^1$ are the direction and magnitude of the q th IF, satisfying $\|\xi_q\| = 1$. Moreover, the active and inactive duration of the q th IF are $\tau_q^o = \nu_q - \mu_q$ and $\tau_q^r = \mu_{q+1} - \nu_q$, respectively. Note that they are counted by sampling intervals here. The q th IF can be denoted by five parameters, i.e., $\text{IF}(\xi_q, f_q, \tau_{q-1}^r, \tau_q^o, \tau_q^r)$.

Remark 2. Recall that the characteristics of IFs are small magnitude and short duration. In most cases, since the fault magnitude is small, when an IF becomes active, after exhibiting a short transient behavior, the system will be driven to another steady state soon by the closed-loop control, instead of being continuously sharp fluctuations or out of control. Similarly, when the IF becomes inactive, after a short transition, the closed-loop control will drive the system back to its normal steady state soon. Moreover, since the fault duration is short, we can assume the fault direction and magnitude within each IF to be constant. Therefore, IFs can be represented by the form of intermittent biases as (11). This statement will be confirmed by a realistic simulation of the practical CSTR benchmark in Section 6.

The fault detectability concept was first defined in [36, 37] within the MSPM framework, and has been widely adopted by a variety of MSPM methods [2, 26, 30, 33] to study the FD performance. However, the concept has been mainly concerned with PFs. Compared with a PFD task, additional requirements for an IFD task [5, 38, 39] are to determine each appearance (disappearance) of an IF before its subsequent disappearance (appearance), otherwise missing or false alarms occur. Following these considerations, this paper extends and generalizes the original fault detectability concept [36] to make it suitable for both PFs and IFs.

Definition 1. For a given significance level α , the disappearance of the q th IF is said to be **guaranteed detectable** (DPG-detectable) by the WMA-TCC(W), if there exists a time instance $\nu_q \leq k^\# < \mu_{q+1}$ such that for each $k^\# \leq k < \mu_{q+1}$, the detection statistic $\tilde{T}_k^2(W) \leq \delta^2$ is guaranteed for all values of \tilde{X}_k^* in (10).

Definition 2. For a given significance level α , the appearance of the q th IF is said to be **guaranteed detectable** (APG-detectable) by the WMA-TCC(W), if the

disappearance of the $(q-1)$ th IF is guaranteed detectable, and there exists a time instance $\mu_q \leq \mathbf{k}^* < \nu_q$ such that for each $k^* \leq \mathbf{k} < \nu_q$, the detection statistic $\tilde{T}_k^2(W) > \delta^2$ is guaranteed for all values of \tilde{X}_k^* in (10).

Definition 3. For a given significance level α , the q th IF is said to be **guaranteed detectable** (G-detectable) by the WMA-TCC(W), if both the appearance and disappearance of the q th IF are guaranteed detectable.

3.2. Detectability conditions

Intuitively, to detect the disappearance/appearance of an IF, we can choose a window length that is no more than the IF's inactive/active duration, so that the WMA-TCC(W) is free from interference of previous faulty/fault-free samples after some delay.

Lemma 2. For the WMA-TCC(W) and a given significance level α , when $W \leq \tau_q^r$, the disappearance of the q th IF is guaranteed detectable (DPG-detectable).

Proof. According to the IF model (11), when $W \leq \tau_q^r$, there exists a time instance $\nu_q \leq \mathbf{k}^\# < \mu_{q+1}$, such that for each $k^\# \leq \mathbf{k} < \mu_{q+1}$, all W current process samples within the time window are fault-free. Then we have $\tilde{X}_k^f = \tilde{X}_k^*$ and

$$\tilde{T}_k^2(W) = \|\tilde{S}_W^{-1/2}(\tilde{X}_k^f - \tilde{X})\|^2 = \|\tilde{S}_W^{-1/2}(\tilde{X}_k^* - \tilde{X})\|^2.$$

Thus, for each $k^\# \leq \mathbf{k} < \mu_{q+1}$, the detection statistic $\tilde{T}_k^2(W) \leq \delta^2$ is guaranteed for all values of \tilde{X}_k^* in (10). \square

Lemma 3. For the WMA-TCC(W) and a given significance level α , when $W \leq \min\{\tau_{q-1}^r, \tau_q^o\}$, the appearance of the q th IF is guaranteed detectable (APG-detectable) if and only if

$$\|\tilde{S}_W^{-1/2}\xi_q f_q\| > 2\delta. \quad (12)$$

Proof. According to Lemma 2, when $W \leq \min\{\tau_{q-1}^r, \tau_q^o\}$, the disappearance of the $(q-1)$ th IF is guaranteed detectable. Moreover, there exists a time instance $\mu_q \leq \mathbf{k}^* < \nu_q$, such that for each $k^* \leq \mathbf{k} < \nu_q$, all W current process samples within the time window are faulty. Then we have $\tilde{X}_k^f = \tilde{X}_k^* + \xi_q f_q$ and

$$\begin{aligned} \tilde{T}_k^2(W) &= \|\tilde{S}_W^{-1/2}(\tilde{X}_k^* - \tilde{X} + \xi_q f_q)\|^2 \\ &\geq \left(\|\tilde{S}_W^{-1/2}\xi_q f_q\| - \|\tilde{S}_W^{-1/2}(\tilde{X}_k^* - \tilde{X})\| \right)^2. \end{aligned} \quad (13)$$

Then by following (12), (10) and (13), we derive that for each $k^* \leq \mathbf{k} < \nu_q$, $\tilde{T}_k^2(W) > \delta^2$ is guaranteed for all values of \tilde{X}_k^* in (10) and the proof of sufficiency is complete.

We now prove the necessity by contraposition. The contrapositive of the necessity statement is: When $W \leq \min\{\tau_{q-1}^r, \tau_q^o\}$, if $\|\tilde{S}_W^{-1/2}\xi_q f_q\| \leq 2\delta$, then the disappearance of the $(q-1)$ th IF is not guaranteed detectable, or for any time instance $\mu_q \leq \mathbf{k}^* < \nu_q$, there exists a time instance $k^* \leq \mathbf{k} < \nu_q$ and a value of \tilde{X}_k^* in (10), making $\tilde{T}_k^2(W) \leq \delta^2$ valid. This contrapositive statement can be proven as follows. For any given $\mu_q \leq \mathbf{k}^* < \nu_q$, we consider time instance $k = \nu_q - 1$ which satisfies $k^* \leq \mathbf{k} < \nu_q$. We further consider the following value of \tilde{X}_k^* : $\tilde{S}_W^{-1/2}(\tilde{X}_k^* - \tilde{X}) = -\tilde{S}_W^{-1/2}\xi_q f_q/2$, which satisfies (10) if $\|\tilde{S}_W^{-1/2}\xi_q f_q\| \leq 2\delta$. Note that at time instance $k = \nu_q - 1$, we have $\tilde{X}_k^f = \tilde{X}_k^* + \xi_q f_q$ and consequently $\tilde{T}_k^2(W) = \|\tilde{S}_W^{-1/2}\xi_q f_q/2\|^2 \leq \delta^2$. Having proven the contrapositive, we infer the original statement and the proof of necessity is complete. \square

Theorem 1. For the WMA-TCC(W) and a given significance level α , when $W \leq W^\# \triangleq \min\{\tau_{q-1}^r, \tau_q^o, \tau_q^r\}$, the q th IF is guaranteed detectable (G-detectable) if and only if inequality (12) holds.

Proof. Directly derived from Lemmas 2 and 3. \square

4. Determination of the weight and window length

In this section, methods to determine the weight vector and window length are provided, along with discussions on the existence, symmetry and uniqueness of the optimal weight.

4.1. Problem formulation and main results

Now, we are in the position to find the optimal weight vector based on the above derived detectability conditions, and present the main problem as follows.

Problem 1. For the WMA-TCC(W), $W \leq W^\#$, find the optimal weight \vec{a}_W^* that

$$\begin{aligned} \max_{\vec{a}_W} \quad & \beta(\vec{a}_W) = \frac{1}{2} \|\tilde{S}_W^{-1/2}\xi_q\|^2, \\ \text{s.t.} \quad & g(\vec{a}_W) = \sum_{j=1}^W a_j = 1. \end{aligned} \quad (14)$$

Theorem 2. The optimal weight \vec{a}_W^* maximizing $\beta(\vec{a}_W)$ of Problem 1 satisfies

$$\hat{\mathcal{T}}(\vec{a}_W^*)\vec{a}_W^* = b, \quad (16)$$

and

$$(-1)^k \left| \overline{\mathcal{H}}_k(\vec{a}_W^*) \right| \geq 0, \quad k = 2, 3, \dots, W, \quad (17)$$

where $\hat{\mathcal{T}}(\vec{a}_W) \in \mathbb{R}^{W \times W}$, $b = [0, \dots, 0, 1]^T \in \mathbb{R}^W$,

$$\begin{aligned} \hat{\mathcal{T}}_{l,j}(\vec{a}_W) &= \begin{cases} \xi_q^T \tilde{S}_W^{-1} (\hat{R}_{lj} - \hat{R}_{(l+1)j}) \tilde{S}_W^{-1} \xi_q, & l < W, \\ 1, & l = W, \end{cases} \\ \hat{R}_{lj} &= \frac{1}{N-1} \sum_{i=1}^N (X_i^l - \bar{X}^l)(X_i^j - \bar{X}^j)^T, \\ \bar{X}^j &= \frac{1}{N} \sum_{i=1}^N X_i^j, \end{aligned} \quad (18)$$

and \tilde{S}_W is short for $\tilde{S}_W(\vec{a}_W)$ calculated by (4),

$$\begin{aligned} |\overline{\mathcal{H}}_k(\vec{a}_W)| &= \begin{vmatrix} 0 & 1 & \cdots & 1 \\ 1 & \hat{H}_{1,1}(\vec{a}_W) & \cdots & \hat{H}_{1,k}(\vec{a}_W) \\ \vdots & \vdots & \ddots & \vdots \\ 1 & \hat{H}_{k,1}(\vec{a}_W) & \cdots & \hat{H}_{k,k}(\vec{a}_W) \end{vmatrix}, \\ \hat{H}_{l,l'}(\vec{a}_W) &= h_l^T h_{l'} - \xi_q^T \tilde{S}_W^{-1} \hat{R}_{ll'} \tilde{S}_W^{-1} \xi_q, \\ \hat{h}_l(\vec{a}_W) &= \tilde{S}_W^{-1/2} \left(\sum_{j=1}^W a_j (\hat{R}_{lj} + \hat{R}_{lj}^T) \right) \tilde{S}_W^{-1} \xi_q. \end{aligned} \quad (19)$$

Proof. For this nonlinear constrained optimization problem, we can construct a Lagrange function given by

$$\mathcal{L}(\vec{a}_W, \lambda) = \frac{1}{2} \|\tilde{S}_W^{-1/2} \xi_q\|^2 + \lambda \left(\sum_{j=1}^W a_j - 1 \right), \quad (20)$$

where λ is a Lagrange multiplier. According to the Karush-Kuhn-Tucker conditions (first-order necessary conditions) [40], the optimal weight \vec{a}_W^* should satisfy

$$\nabla_{\vec{a}_W} \mathcal{L}(\vec{a}_W, \lambda) = 0_W, \quad \nabla_{\lambda} \mathcal{L}(\vec{a}_W, \lambda) = 0. \quad (21)$$

Note that

$$\begin{aligned} \frac{\partial \mathcal{L}(\vec{a}_W, \lambda)}{\partial a_l} &= -\frac{1}{2} \xi_q^T \tilde{S}_W^{-1} \left(\frac{\partial \tilde{S}_W}{\partial a_l} \right) \tilde{S}_W^{-1} \xi_q + \lambda \\ &= -\xi_q^T \tilde{S}_W^{-1} \left(\sum_{j=1}^W a_j \hat{R}_{lj} \right) \tilde{S}_W^{-1} \xi_q + \lambda. \end{aligned} \quad (22)$$

By setting the above derivative of $\mathcal{L}(\vec{a}_W, \lambda)$ with respect to \vec{a}_W to zeros, the following equations can be obtained.

$$\xi_q^T \tilde{S}_W^{-1} \left(\sum_{j=1}^W a_j (\hat{R}_{lj} - \hat{R}_{l'j}) \right) \tilde{S}_W^{-1} \xi_q = 0, \quad 1 \leq l, l' \leq W. \quad (23)$$

Thus, integrating (23) with (15), the first-order necessary conditions for the constrained optimization problem are derived as (16).

When \vec{a}_W^* meets (16), it is considered an extremum point or saddle point for function (14) subject to constraint (15). According to [41], second-order necessary conditions for \vec{a}_W^* to be a maximum point are: the leading principal minors of $\overline{\mathcal{H}}(\vec{a}_W^*)$ of order $k+1$ ($k=2, 3, \dots, W$) have sign $(-1)^k$ or equal to zero, where

$$\overline{\mathcal{H}}(\vec{a}_W) = \begin{bmatrix} 0 & \nabla_{\vec{a}_W}^T g(\vec{a}_W) \\ \nabla_{\vec{a}_W} g(\vec{a}_W) & \hat{H}(\vec{a}_W) \end{bmatrix}, \quad (24)$$

is a bordered Hessian matrix and

$$\hat{H}(\vec{a}_W) = \nabla_{\vec{a}_W}^2 \mathcal{L}(\vec{a}_W, \lambda), \quad \text{i.e. } \hat{H}_{l,l'}(\vec{a}_W) = \frac{\partial^2 \mathcal{L}(\vec{a}_W, \lambda)}{\partial a_l \partial a_{l'}}.$$

Thus, the second-order necessary conditions for the optimization problem are derived as (17). \square

4.2. Existence of the solution

In this subsection, we prove the existence of the solution of nonlinear equations (16) with the help of the well-known Brouwer fixed-point theory. We begin with the following assumption and the result is given in *Theorem 3* at last. Additionally, methods to obtain the optimal weight are discussed and a bound of the optimal weight is given.

Assumption 1. $\hat{\Gamma}^W$ is nonsingular, where

$$\hat{\Gamma}^k = \begin{bmatrix} \hat{R}_{11} & \hat{R}_{12} & \cdots & \hat{R}_{1k} \\ \hat{R}_{21} & \hat{R}_{22} & \cdots & \hat{R}_{2k} \\ \vdots & \vdots & \ddots & \vdots \\ \hat{R}_{k1} & \hat{R}_{k2} & \cdots & \hat{R}_{kk} \end{bmatrix} \in \mathbb{R}^{pk \times pk}. \quad (25)$$

Remark 3. Assumption 1 is the same as the assumption for Yule-Walker equations, which are well-known in the field of parameter identification of time series models. In real applications, Assumption 1 holds due to the existence of process and measurement noises.

Proposition 1. Suppose Assumption 1 holds, then $\tilde{S}_W(\vec{a}_W)$ and $\hat{\mathcal{T}}(\vec{a}_W)$ are nonsingular, if $\vec{a}_W \neq 0_W$ and $\|\vec{a}_W\| < \infty$.

Proof. Let $\varepsilon_i^j = X_i^j - \bar{X}^j$. Then, we can rewrite $\hat{\Gamma}^k = \frac{1}{N-1} \hat{\Upsilon}_k \hat{\Upsilon}_k^T$, where $\hat{\Upsilon}_k \in \mathbb{R}^{pk \times N}$ and

$$\hat{\Upsilon}_k = \begin{bmatrix} \varepsilon_1^1 & \varepsilon_2^1 & \cdots & \varepsilon_N^1 \\ \varepsilon_1^2 & \varepsilon_2^2 & \cdots & \varepsilon_N^2 \\ \vdots & \vdots & \ddots & \vdots \\ \varepsilon_1^k & \varepsilon_2^k & \cdots & \varepsilon_N^k \end{bmatrix}.$$

Thus, $\hat{\Gamma}^k$ is positive semidefinite. Moreover, by following *Assumption 1*, we know that $\hat{\Gamma}^W$ is positive definite. According to (4) and (18), we have

$$\begin{aligned}\tilde{S}_W(\vec{a}_W) &= \frac{1}{N-1} \sum_{k=1}^N (\tilde{X}_k - \bar{X})(\tilde{X}_k - \bar{X})^T \\ &= \frac{1}{N-1} \sum_{k=1}^N \left[\sum_{i=1}^W a_i (X_k^i - \frac{1}{N} \sum_{l=1}^N X_l^i) \right] \left[\sum_{j=1}^W a_j (X_k^j - \frac{1}{N} \sum_{l=1}^N X_l^j) \right]^T \\ &= \frac{1}{N-1} \sum_{k=1}^N \sum_{i=1}^W \sum_{j=1}^W a_i a_j (X_k^i - \bar{X}^i)(X_k^j - \bar{X}^j)^T \\ &= \sum_{i=1}^W \sum_{j=1}^W a_i a_j \hat{R}_{ij} = (\vec{a}_W \otimes I_p)^T \hat{\Gamma}^W (\vec{a}_W \otimes I_p).\end{aligned}\quad (26)$$

For any $\vec{a}_W \neq 0_W$, the matrix $\vec{a}_W \otimes I_p$ is full column rank. Thus, $\tilde{S}_W(\vec{a}_W)$ is nonsingular, and

$$0 < \lambda_{\min}(\hat{\Gamma}^W) \|\vec{a}_W\|^2 I_p \leq \tilde{S}_W \leq \lambda_{\max}(\hat{\Gamma}^W) \|\vec{a}_W\|^2 I_p. \quad (27)$$

Let $\hat{\gamma}^W \in \mathbb{R}^{W \times W}$ be the abbreviation of $\hat{\gamma}^W(\vec{a}_W)$, and define

$$\hat{\gamma}_{l,j}^W = \xi_q^T \tilde{S}_W^{-1} \hat{R}_{lj} \tilde{S}_W^{-1} \xi_q. \quad (28)$$

Then, it follows from *Assumption 1* and (27) that, for any $\vec{a}_W \neq 0_W$ and $\|\vec{a}_W\| < \infty$,

$$\hat{\gamma}^W = (I_W \otimes \tilde{S}_W^{-1} \xi_q)^T \hat{\Gamma}^W (I_W \otimes \tilde{S}_W^{-1} \xi_q),$$

is nonsingular and positive definite. By following a few reformulations, we can rewrite $\hat{\mathcal{T}}(\vec{a}_W) = \hat{J} \hat{\gamma}^W$, where

$$\hat{J} = \begin{bmatrix} 1 & -1 & 0 & \cdots & 0 \\ 0 & 1 & -1 & \ddots & \vdots \\ \vdots & \ddots & \ddots & \ddots & 0 \\ 0 & \cdots & 0 & 1 & -1 \\ \hline & & & & 1_W^T (\hat{\gamma}^W)^{-1} \end{bmatrix} \in \mathbb{R}^{W \times W}.$$

Thus, $\hat{\mathcal{T}}(\vec{a}_W)$ is nonsingular if and only if \hat{J} is nonsingular. We assume that \hat{J} is singular, then there exists $\vec{\alpha}_W = [\alpha_1, \alpha_2, \dots, \alpha_W]^T \neq 0_W$, such that

$$\alpha_1 \hat{J}_{1,:} + \alpha_2 \hat{J}_{2,:} + \cdots + \alpha_{W-1} \hat{J}_{W-1,:} + \alpha_W \hat{J}_{W,:} = 0_W^T.$$

Multiplying both sides by 1_W on the right, we have $\alpha_W 1_W^T (\hat{\gamma}^W)^{-1} 1_W = 0$. Since $\hat{\gamma}^W$ is positive definite, we obtain $\alpha_W = 0$. This means that the first $W-1$ rows of \hat{J} are linearly dependent, which contradicts the fact that $\hat{J}_{W \setminus \emptyset}$ has full row rank. Thus, \hat{J} is nonsingular and the

proof is complete. \square

Remark 4. According to *Proposition 1*, we can rewrite

$$\vec{a}_W^* = \hat{\mathcal{T}}^{-1}(\vec{a}_W^*) b \triangleq \hat{\mathcal{F}}(\vec{a}_W^*) \in \mathbb{R}^W. \quad (29)$$

It can be seen that \vec{a}_W^* is a fixed-point of function $\hat{\mathcal{F}}$. According to our practical experience, \vec{a}_W^* can be obtained by successive approximations as follows

$$\vec{a}_W^{k+1} = \hat{\mathcal{F}}(\vec{a}_W^k), \quad \forall \vec{a}_W^0 \neq 0_W, \|\vec{a}_W^0\| < \infty. \quad (30)$$

Since $\hat{\mathcal{F}}(\vec{a}_W^k) \neq 0_W$ and $\|\hat{\mathcal{F}}(\vec{a}_W^k)\| < \infty$, *Propositions 1 and 2* guarantee this process is always implementable. Moreover, it follows from (27) that $\lim_{\|\vec{a}_W\| \rightarrow \infty} \beta(\vec{a}_W) = 0$. Thus, although any \vec{a}_W such that $\|\vec{a}_W\| = \infty$ and $g(\vec{a}_W) = 1$ satisfies (16), it is not the solution of *Problem 1*.

Lemma 4. For any column vectors x, y and matrix $P \geq 0$, the following inequality holds:

$$2\|x^T P y\| \leq x^T P x + y^T P y. \quad (31)$$

Proof. Directly derived from $0 \leq (x-y)^T P (x-y)$ and $0 \leq (x+y)^T P (x+y)$. \square

Proposition 2. Suppose *Assumption 1* holds, then $\|\hat{\mathcal{F}}(\vec{a}_W)\|_\infty \leq \frac{W+1}{2W} \frac{\lambda_{\max}(\hat{\Gamma}^W)}{\lambda_{\min}(\hat{\Gamma}^W)} \triangleq d_W$ and $g(\hat{\mathcal{F}}(\vec{a}_W)) = 1$, if $\vec{a}_W \neq 0_W$ and $\|\vec{a}_W\| < \infty$.

Proof. Let $\vec{c}_W = [c_1, \dots, c_W]^T$, according to (29), we have

$$\hat{\mathcal{F}}(\vec{a}_W) = |\hat{\mathcal{T}}(\vec{a}_W)|^{-1} \text{adj}(\hat{\mathcal{T}}(\vec{a}_W)) b = |\hat{\mathcal{T}}(\vec{a}_W)|^{-1} \vec{c}_W, \quad (32)$$

with $c_i = (-1)^{W+i} |\hat{\mathcal{T}}_{W \setminus i}(\vec{a}_W)| = |\check{\mathcal{T}}(\vec{a}_W, i)|$, where

$$\check{\mathcal{T}}_{l,j}(\vec{a}_W, i) = \begin{cases} \hat{\mathcal{T}}_{l,j}(\vec{a}_W), & l < W, \\ \delta_{ij}, & l = W. \end{cases} \quad (33)$$

Note that $g(\vec{c}_W) = |\hat{\mathcal{T}}(\vec{a}_W)|$. Thus, $g(\hat{\mathcal{F}}(\vec{a}_W)) = |\hat{\mathcal{T}}(\vec{a}_W)|^{-1} g(\vec{c}_W) = 1$. Moreover, by following a few reformulations, we can rewrite $\check{\mathcal{T}}(\vec{a}_W, i) = \check{J}^i \hat{\gamma}^W$, where

$$\check{J}^i = \begin{bmatrix} 1 & -1 & 0 & \cdots & 0 \\ 0 & 1 & -1 & \ddots & \vdots \\ \vdots & \ddots & \ddots & \ddots & 0 \\ 0 & \cdots & 0 & 1 & -1 \\ \hline & & & & e_{Wi}^T (\hat{\gamma}^W)^{-1} \end{bmatrix} \in \mathbb{R}^{W \times W}.$$

Note that $0 < \lambda_{\min}(\hat{\Gamma}^W) I_{pW} \leq \hat{\Gamma}^W \leq \lambda_{\max}(\hat{\Gamma}^W) I_{pW}$. Then

$$0 < \lambda_{\min}(\hat{\Gamma}^W) \varrho(\vec{a}_W) I_W \leq \hat{\gamma}^W \leq \lambda_{\max}(\hat{\Gamma}^W) \varrho(\vec{a}_W) I_W,$$

where $\varrho(\vec{a}_W) = \xi_q^T \tilde{\Sigma}_W^{-2} \xi_q$. For $|\hat{J}|$ and $|\hat{J}^i|$, adding its j th column to its $j-1$ th column in turn, we obtain $|\hat{J}| = 1_W^T (\hat{\gamma}^W)^{-1} 1_W$ and $|\hat{J}^i| = e_{Wi}^T (\hat{\gamma}^W)^{-1} 1_W$. Note that

$$\frac{W}{\lambda_{\max}(\hat{\Gamma}^W)\varrho(\vec{a}_W)} \leq |\hat{J}| = 1_W^T (\hat{\gamma}^W)^{-1} 1_W \leq \frac{W}{\lambda_{\min}(\hat{\Gamma}^W)\varrho(\vec{a}_W)},$$

$$\frac{1}{\lambda_{\max}(\hat{\Gamma}^W)\varrho(\vec{a}_W)} \leq e_{Wi}^T (\hat{\gamma}^W)^{-1} e_{Wi} \leq \frac{1}{\lambda_{\min}(\hat{\Gamma}^W)\varrho(\vec{a}_W)}.$$

Then, according to Lemma 4, we have

$$\|c_i\| = \left\| |\hat{J}^i| \|\hat{\gamma}^W\| \right\| \leq \frac{1}{2} \left(e_{Wi}^T (\hat{\gamma}^W)^{-1} e_{Wi} + |\hat{J}| \right) \|\hat{\gamma}^W\|$$

$$\leq \frac{W+1}{2\lambda_{\min}(\hat{\Gamma}^W)\varrho(\vec{a}_W)} \|\hat{\gamma}^W\|.$$

For the i th element of $\hat{\mathcal{F}}(\vec{a}_W)$, we have

$$\|\hat{\mathcal{F}}_i(\vec{a}_W)\| = \frac{\|c_i\|}{|\hat{J}|\|\hat{\gamma}^W\|} \leq \frac{W+1}{2W} \frac{\lambda_{\max}(\hat{\Gamma}^W)}{\lambda_{\min}(\hat{\Gamma}^W)}.$$

Note that $\|\hat{\mathcal{F}}(\vec{a}_W)\|_\infty = \max_{i=1,\dots,W} \|\hat{\mathcal{F}}_i(\vec{a}_W)\|$, then the proof is complete. \square

Remark 5. Proposition 2 presents a bound of the optimal weight, i.e., $\vec{a}_W^* \in \mathcal{M}_W$ given in (34). Moreover, Proposition 2 further guarantees the iteration process (30) is always bounded. In the following, we give the well-known Brouwer fixed-point theorem.

Lemma 5. [42] Suppose that M is a nonempty, convex, compact subset of \mathbb{R}^n , where $n \geq 1$, and that $\mathcal{F} : M \rightarrow M$ is a continuous mapping. Then \mathcal{F} has a fixed point.

Theorem 3. Suppose Assumption 1 holds, then the nonlinear equations (16) have a solution.

Proof. Define a subset of \mathbb{R}^W as

$$\mathcal{M}_W = \{\vec{a}_W \in \mathbb{R}^W : g(\vec{a}_W) = 1, \|\vec{a}_W\|_\infty \leq d_W\}, \quad (34)$$

and let $\vec{a}_W^x, \vec{a}_W^y \in \mathcal{M}_W$. Then for any $0 \leq \theta \leq 1$, we have $\vec{a}_W^z = \theta \vec{a}_W^x + (1-\theta)\vec{a}_W^y \in \mathcal{M}_W$, which means the set \mathcal{M}_W is convex. This can be seen by

$$g(\vec{a}_W^z) = \theta g(\vec{a}_W^x) + (1-\theta)g(\vec{a}_W^y) = 1,$$

$$\|\vec{a}_W^z\|_\infty \leq \theta \|\vec{a}_W^x\|_\infty + (1-\theta)\|\vec{a}_W^y\|_\infty \leq d_W.$$

Since \mathcal{M}_W is closed and bounded in the finite dimensional normed space \mathbb{R}^W , it is compact. Moreover, for any $\vec{a}_W^0 \in \mathcal{M}_W$, $\hat{\mathcal{F}}(\vec{a}_W) \rightarrow \hat{\mathcal{F}}(\vec{a}_W^0)$ as $\vec{a}_W \rightarrow \vec{a}_W^0$. Thus, $\hat{\mathcal{F}}(\vec{a}_W)$ is continuous on \mathcal{M}_W . According to Proposition 2, we have $\hat{\mathcal{F}}(\mathcal{M}_W) \subseteq \mathcal{M}_W$, where $\hat{\mathcal{F}}(\mathcal{M}_W)$ is

the images of \mathcal{M}_W . Now $\hat{\mathcal{F}}$ is a continuous map of the nonempty, convex, compact set \mathcal{M}_W into itself. By Lemma 5, there exists a fixed point for $\hat{\mathcal{F}}$ and consequently the nonlinear equations (16) have a solution. \square

4.3. Symmetry of the optimal weight

Intuitively, since the process is stationary, the first and last samples in a time window always have the same contributions to the covariance matrix $\tilde{\Sigma}_W$, as can be seen in (5). Therefore, they should have the same weight when N is sufficiently large. This is also true for the second and the penultimate samples, and so on. In this subsection, we reveal that the optimal weight possesses a symmetrical structure, see Theorem 4.

Proposition 3. When N is sufficiently large, we have

$$\mathbb{E}(\hat{R}_{l_j}) = R_{l-j}, \quad \lim_{N \rightarrow \infty} \hat{R}_{l_j} = R_{l-j}, a.s. \quad (35)$$

$$\mathbb{E}(\tilde{S}_W) = \tilde{\Sigma}_W, \quad \lim_{N \rightarrow \infty} \tilde{S}_W = \tilde{\Sigma}_W, a.s. \quad (36)$$

Proof. According to (26), we can derive (36) directly if (35) holds. As for (35), note that $X_{i_1}^{j_1}$ and $X_{i_2}^{j_2}$ are independent for $i_1 \neq i_2$. Thus, $\mathbb{E}(X_{i_1}^{j_1}(\bar{X}^{j_2})^T) = \mathbb{E}(\bar{X}^{j_1}(X_{i_1}^{j_2})^T) = \frac{1}{N}R_{l-j} + \mu\mu^T$ and $\mathbb{E}(\bar{X}^{j_1}(\bar{X}^{j_2})^T) = \frac{1}{N}R_{l-j} + \mu\mu^T$. Then

$$\mathbb{E}(\hat{R}_{l_j}) = \frac{1}{N-1} \sum_{i=1}^N \mathbb{E} \left[X_i^l (X_i^j)^T - X_i^l (\bar{X}^j)^T \right. \\ \left. - \bar{X}^l (X_i^j)^T + \bar{X}^l (\bar{X}^j)^T \right] = R_{l-j}.$$

Moreover, it is well known that the stationary Gaussian process is ergodic. Thus,

$$\lim_{N \rightarrow \infty} \bar{X}^j = \lim_{N \rightarrow \infty} \frac{1}{N} \sum_{i=1}^N X_i^j = \mathbb{E}(X_i^j) = \mu, a.s.,$$

$$\lim_{N \rightarrow \infty} \frac{1}{N-1} \sum_{i=1}^N X_i^l (X_i^j)^T = \mathbb{E}(X_i^l (X_i^j)^T) = R_{l-j} + \mu\mu^T, a.s.$$

Substituting them into (18), we derive (35). \square

Theorem 4. Suppose Assumption 1 holds and N is sufficient large, then the optimal weight \vec{a}_W^* maximizing $\beta(\vec{a}_W)$ of Problem 1 satisfies

$$a_j^* = a_{W-j+1}^*, \quad 1 \leq j \leq W. \quad (37)$$

Proof. According to Proposition 3, when N is sufficiently large, we almost surely have

$$\mathcal{T}_{l,j} = \begin{cases} \xi_q^T \tilde{\Sigma}_W^{-1} (R_{l-j} - R_{l+1-j}) \tilde{\Sigma}_W^{-1} \xi_q, & l < W, \\ 1, & l = W, \end{cases}$$

where \mathcal{T} is short for $\mathcal{T}(\vec{a}_W)$, such that

$$\mathcal{T}(\vec{a}_W^*)\vec{a}_W^* = b. \quad (38)$$

Following $R_{-l} = R_l^T$, it can be seen that

$$\begin{aligned} \mathcal{T}_{l,j} &= \mathcal{T}_{l+1,j+1}, & l < W-1, j < W, \\ \mathcal{T}_{l,j} &= -\mathcal{T}_{j-1,l}, & l \leq W-1, j \leq W. \end{aligned}$$

Denote $A_{\setminus l \setminus \emptyset}$ and $A_{\setminus \emptyset \setminus j}$ as the matrices obtained from A by deleting the l th row and j th column, respectively. Then, $\mathcal{T}_{\setminus W \setminus \emptyset} \in \mathbb{R}^{W-1 \times W}$ has the following form

$$\mathcal{T}_{\setminus W \setminus \emptyset} = \begin{bmatrix} -t_1 & t_1 & t_2 & \cdots & t_{W-2} & t_{W-1} \\ -t_2 & -t_1 & t_1 & t_2 & \ddots & t_{W-2} \\ -t_3 & -t_2 & -t_1 & t_1 & \ddots & \vdots \\ \vdots & \ddots & \ddots & \ddots & \ddots & t_2 \\ -t_{W-1} & \cdots & -t_3 & -t_2 & -t_1 & t_1 \end{bmatrix},$$

where $t_l = \xi_q^T \tilde{\Sigma}_W^{-1} (R_{-l} - R_{1-l}) \tilde{\Sigma}_W^{-1} \xi_q$, and is an abbreviation for $t_l(\vec{a}_W)$. Define $\text{cen}(A) \in \mathbb{R}^{m \times n}$ as the centrosymmetry of a matrix $A \in \mathbb{R}^{m \times n}$, namely, $[\text{cen}(A)]_{l,j} = [A]_{m-l+1, n-j+1}$. It can be easily verified that the operator $\text{cen}()$ has the following properties:

$$\text{cen}(\text{cen}(A)) = A, \quad \text{cen}(-A) = -\text{cen}(A). \quad (39)$$

Besides, if A is a square matrix, then we have $|\text{cen}(A)| = |A|$. Moreover, if A is centrosymmetric, that is to say, $\text{cen}(A) = A$, then we have

$$\text{cen}(A_{\setminus \emptyset \setminus j}) = A_{\setminus \emptyset \setminus n-j+1}. \quad (40)$$

Note that $[\mathcal{T}_{\setminus W \setminus \emptyset}]_{l,j} = -[\mathcal{T}_{\setminus W \setminus \emptyset}]_{W-l, W-j+1}$, i.e. $\text{cen}(\mathcal{T}_{\setminus W \setminus \emptyset}) = -\mathcal{T}_{\setminus W \setminus \emptyset}$. According to (39) and (40), we have

$$\text{cen}(\mathcal{T}_{\setminus W \setminus j}) = -\mathcal{T}_{\setminus W \setminus W-j+1}. \quad (41)$$

Thus,

$$|\mathcal{T}_{\setminus W \setminus j}| = |-\text{cen}(\mathcal{T}_{\setminus W \setminus W-j+1})| = (-1)^{W-1} |\mathcal{T}_{\setminus W \setminus W-j+1}|.$$

Since $\mathcal{T}(\vec{a}_W)$ is nonsingular for any weight vector $\vec{a}_W \neq 0_W$, similar to the Cramer's rule, we have $\vec{a}_W^* = \mathcal{T}^{-1}(\vec{a}_W^*)b = |\mathcal{T}(\vec{a}_W^*)|^{-1} \text{adj}(\mathcal{T}(\vec{a}_W^*))b$. Then

$$\begin{aligned} a_j^* &= (-1)^{W+j} |\mathcal{T}(\vec{a}_W^*)|^{-1} |\mathcal{T}_{\setminus W \setminus j}(\vec{a}_W^*)| \\ &= (-1)^{2W-j+1} |\mathcal{T}(\vec{a}_W^*)|^{-1} |\mathcal{T}_{\setminus W \setminus W-j+1}(\vec{a}_W^*)| = a_{W-j+1}^*, \end{aligned}$$

which completes the proof. \square

4.4. Further results in several special cases

Note that *Theorem 2* only gives the necessary conditions. Nevertheless, in some special cases, we can further find necessary and sufficient conditions, and determine the optimal weight exactly.

Proposition 4. *If \vec{a}_W^* meets (16) and makes the strict inequality in (17) hold, then it is a maximum point of $\beta(\vec{a}_W)$ in Problem 1.*

Proof. According to [41], when \vec{a}_W^* meets the first-order necessary conditions (16), the second-order sufficient conditions for \vec{a}_W^* to be a maximum point (rather than a minimum or saddle point) are: the leading principal minors of $\overline{\mathcal{H}}(\vec{a}_W^*)$ of order $k+1$ ($k=2, 3, \dots, W$) have sign $(-1)^k$. By following *Theorem 2*, we obtain this proposition. \square

Proposition 5. *For the optimal weight \vec{a}_W^* maximizing $\beta(\vec{a}_W)$ of Problem 1, we have*

$$2\beta(\vec{a}_W^*) = \hat{\gamma}_{l,:}^W(\vec{a}_W^*)\vec{a}_W^*, \quad 1 \leq l \leq W. \quad (42)$$

Proof. It follows from (26) that

$$\begin{aligned} \|\tilde{\mathcal{S}}_W^{-1/2} \xi_q\|^2 &= \xi_q^T \tilde{\mathcal{S}}_W^{-1} (\vec{a}_W \otimes I_p)^T \hat{\Gamma}_W (\vec{a}_W \otimes I_p) \tilde{\mathcal{S}}_W^{-1} \xi_q \\ &= (\vec{a}_W \otimes \tilde{\mathcal{S}}_W^{-1} \xi_q)^T \hat{\Gamma}_W (\vec{a}_W \otimes \tilde{\mathcal{S}}_W^{-1} \xi_q) \\ &= \vec{a}_W^T (I_W \otimes \tilde{\mathcal{S}}_W^{-1} \xi_q)^T \hat{\Gamma}_W (I_W \otimes \tilde{\mathcal{S}}_W^{-1} \xi_q) \vec{a}_W = \vec{a}_W^T \hat{\gamma}_{l,:}^W \vec{a}_W. \end{aligned}$$

Note that we have $\hat{\gamma}_{l,:}^W(\vec{a}_W^*)\vec{a}_W^* = \hat{\gamma}_{l',:}^W(\vec{a}_W^*)\vec{a}_W^*$ from (16). Thus,

$$\begin{aligned} 2\beta(\vec{a}_W^*) &= \|\tilde{\mathcal{S}}_W^{-1/2}(\vec{a}_W^*)\xi_q\|^2 = (\vec{a}_W^*)^T \hat{\gamma}^W(\vec{a}_W^*) \\ &= (\vec{a}_W^*)^T [\hat{\gamma}_{1,:}^W(\vec{a}_W^*), \dots, \hat{\gamma}_{:,l}^W(\vec{a}_W^*)] \vec{a}_W^* = (\vec{a}_W^*)^T \hat{\gamma}_{:,l}^W(\vec{a}_W^*). \end{aligned}$$

The last equality is because $1_W^T \vec{a}_W^* = 1$. Then by following $(\hat{\gamma}_{:,l}^W)^T = \hat{\gamma}_{l,:}^W$, we obtain (42). \square

Theorem 5. *When process data are independent, R_0 is nonsingular and N is sufficiently large, the optimal weight \vec{a}_W^* maximizing $\beta(\vec{a}_W)$ of Problem 1 is uniquely determined as*

$$a_1^* = a_2^* = \dots = a_W^* = 1/W. \quad (43)$$

Proof. When process data are independent, we have $R_l = 0, \forall l \neq 0$. By following the proof of *Theorem 4*,

when N is sufficiently large, we almost surely have

$$\mathcal{T}(\vec{a}_W) = \begin{bmatrix} t_0 & -t_0 & 0 & \cdots & 0 \\ 0 & t_0 & -t_0 & \ddots & \vdots \\ \vdots & \ddots & \ddots & \ddots & 0 \\ 0 & \cdots & 0 & t_0 & -t_0 \\ 1 & \cdots & 1 & \cdots & 1 \end{bmatrix}, \quad (44)$$

where $t_0 = \xi_q^T \tilde{\Sigma}_W^{-1} R_0 \tilde{\Sigma}_W^{-1} \xi_q > 0$. Note that

$$|\mathcal{T}(\vec{a}_W)| = W(t_0)^{W-1}, \quad |\mathcal{T}_{\setminus W \setminus j}(\vec{a}_W)| = (-1)^{W-j} (t_0)^{W-1}.$$

Thus, $a_j^* = (-1)^{W+j} |\mathcal{T}(\vec{a}_W^*)|^{-1} |\mathcal{T}_{\setminus W \setminus j}(\vec{a}_W^*)| = 1/W$. Then, $\tilde{\Sigma}_W(\vec{a}_W^*) = \frac{1}{W} R_0$. Substituting them into (19), we have $\hat{H}_{l,l}(\vec{a}_W^*) \rightarrow H_{l,l}(\vec{a}_W^*) = 4W\vartheta - W^2\vartheta\delta_{ll}$ almost surely when N is sufficiently large, where $\vartheta = \xi_q^T R_0^{-1} \xi_q$. Thus,

$$\left| \overline{\mathcal{H}}_k(\vec{a}_W^*) \right| = \begin{vmatrix} 0 & 1_k^T \\ 1_k & -(W^2\vartheta)I_k \end{vmatrix} = k(-1)^k (W^2\vartheta)^{k-1}.$$

Following Proposition 4, (43) is the optimal weight. \square

Theorem 6. Suppose Assumption 1 holds and N is sufficient large, if the optimal weight \vec{a}_W^* maximizing $\beta(\vec{a}_W)$ of Problem 1 is (43), then

$$\xi_q^T \tilde{\Sigma}_W^{-1} \left(\frac{1}{W} \right) (R_j - R_{W-j}) \tilde{\Sigma}_W^{-1} \left(\frac{1}{W} \right) \xi_q = 0, \quad 1 \leq j \leq W-1. \quad (45)$$

Proof. By substituting (43), i.e., $\vec{a}_W^* = \frac{1}{W}$, into (38), we have

$$\sum_{l=j+1}^{W-j} t_l \left(\frac{1}{W} \right) = 0, \quad j = 1, 2, \dots, \left[\frac{W-1}{2} \right]^-,$$

which is equivalent to (45). Here, $[x]^-$ represents the maximum integer no more than x . \square

Remark 6. Theorem 5 explains why the MA scheme, i.e., the equally weighted scheme, is always adopted in FD tasks where samples are assumed to be independent, such as in [25, 26, 28]. Note that when process data are independent, (45) holds since $R_l = 0, \forall l \neq 0$. Theorem 6 further gives a necessary condition for the MA scheme to be optimal. The essence that the equally weighted scheme does not effectively utilize the correlation information of samples is revealed here. When $p = 1$, (45) becomes a necessary and sufficient condition and is equivalent to $R_j = R_{W-j}, 1 \leq j \leq W-1$. This means that in the unidimensional case, the MA scheme is optimal only for special stationary processes that have periodicity.

Theorem 7. When $p = 1$, suppose Assumption 1 holds, then the optimal weight \vec{a}_W^* maximizing $\beta(\vec{a}_W)$ of Problem 1 is uniquely determined as

$$\vec{a}_W^* = \hat{A}^{-1} b, \quad (46)$$

where

$$\hat{A}_{l,j} = \begin{cases} \hat{R}_{lj} - \hat{R}_{(l+1)j}, & l < W, \\ 1, & l = W. \end{cases} \quad (47)$$

Proof. When $p = 1$, we have $\xi_q = 1$, and $\tilde{S}_W(\vec{a}_W)$ is a scalar. Thus, (16) degenerates into linear equations with unique solutions (46). It follows from Proposition 5 that

$$2\beta(\vec{a}_W^*) = \tilde{S}_W^{-1}(\vec{a}_W^*) = \hat{\gamma}_{l,:}^W(\vec{a}_W^*) \vec{a}_W^*, \quad 1 \leq l \leq W. \quad (48)$$

Multiplying both sides by $\tilde{S}_W^2(\vec{a}_W^*)$ and following (28), we obtain $\tilde{S}_W(\vec{a}_W^*) = \hat{\Gamma}_{l,:}^W \vec{a}_W^*$. Substituting it into (19), we have

$$\hat{H}_{l,l}(\vec{a}_W^*) = 4\tilde{S}_W^{-1}(\vec{a}_W^*) - \tilde{S}_W^{-2}(\vec{a}_W^*) \hat{R}_{ll},$$

and thus,

$$\begin{aligned} \left| \overline{\mathcal{H}}_k(\vec{a}_W^*) \right| &= \begin{vmatrix} 0 & 1_k^T \\ 1_k & \tilde{S}_W^{-2}(\vec{a}_W^*) \hat{\Gamma}^k \end{vmatrix} \\ &= (-1)^k \left(\tilde{S}_W^2(\vec{a}_W^*) 1_k^T (\hat{\Gamma}^k)^{-1} 1_k \right) \left| \tilde{S}_W^{-2}(\vec{a}_W^*) \hat{\Gamma}^k \right|. \end{aligned}$$

Note that $\tilde{S}_W, \hat{\Gamma}^k$ are positive definite, then

$$(-1)^k \left| \overline{\mathcal{H}}_k(\vec{a}_W^*) \right| > 0, \quad k = 2, 3, \dots, W.$$

Following Proposition 4, (46) is the optimal weight. \square

Theorem 8. When $W = 2$, suppose Assumption 1 holds and N is sufficiently large, then the optimal weight \vec{a}_W^* maximizing $\beta(\vec{a}_W)$ of Problem 1 is uniquely determined as

$$a_1^* = a_2^* = 1/2. \quad (49)$$

Proof. When $W = 2$, (49) can be derived directly from Theorem 4. When N is sufficiently large, we have

$$\hat{h}_l(\vec{a}_W) \rightarrow h_l(\vec{a}_W) = \tilde{\Sigma}_W^{-1/2} \left(\sum_{j=1}^W a_j (R_{l-j} + R_{l-j}^T) \right) \tilde{\Sigma}_W^{-1} \xi_q.$$

Note that when $W = 2$, we have $h_1(\vec{a}_2^*) = h_2(\vec{a}_2^*)$. Thus,

$$\left| \overline{\mathcal{H}}_k(\vec{a}_2^*) \right| = \begin{vmatrix} 0 & 1_k^T \\ 1_k & -\hat{\gamma}^k \end{vmatrix} = (-1)^k \left(1_k^T (\hat{\gamma}^k)^{-1} 1_k \right) |\hat{\gamma}^k|.$$

Following Proposition 4, (49) is the optimal weight. \square

Remark 7. Note that the derived weights (43), (46) and (49) are optimal regardless of the direction of IFs in these three cases, respectively.

4.5. Selection of the window length

One drawback of introducing a time window is that it causes detection delays. Generally speaking, an over-large window length may incur serious detection delays. As a result, we suggest choosing the smallest window length that guarantees the detection of IFs.

Theorem 9. For the OWMA-TCC with $W \leq W^\#$ and a given significance level α , the q th IF is guaranteed detectable (G-detectable) if and only if

$$\beta(\tilde{a}_{W^\#}^*)f_q^2 > 2\delta^2. \quad (50)$$

Then the window length W can be chosen such that $W^\# \geq W \geq W^*$, where

$$W^* = \arg \min_W \beta(\tilde{a}_W^*)f_q^2 > 2\delta^2. \quad (51)$$

Proof. Note that $\beta([\tilde{a}_{W-1}^*; 0]) \leq \beta(\tilde{a}_W^*)$. Thus, we can conclude that when $W \leq W^\#$, the maximum of $\beta(\tilde{a}_W)$ achieves with $W = W^\#$ and $\tilde{a}_W = \tilde{a}_{W^\#}^*$. Then, this theorem holds according to Theorem 1. \square

In (51), W^* can be solved by exhaustive search from $W = 1$ to $W^\#$. Since larger window length always incurs larger detection delays, we can select W^* as the optimal window length and $\tilde{a}_{W^*}^*$ as the optimal weight vector. In practice, IFs' parameters may not be known exactly, but in most cases lower bounds of fault parameters are available through expert knowledge or analyzing historical data and operating conditions. Denote $\tilde{f}_q, \tilde{\tau}_{q-1}^r, \tilde{\tau}_q^o, \tilde{\tau}_q^r$ as the lower bounds of $f_q, \tau_{q-1}^r, \tau_q^o, \tau_q^r$, respectively. Then we have the following corollaries.

Corollary 1. For the WMA-TCC(W) and a given significance level α , when $W \leq \tilde{W}^\# \triangleq \min\{\tilde{\tau}_{q-1}^r, \tilde{\tau}_q^o, \tilde{\tau}_q^r\}$, the q th IF is guaranteed detectable (G-detectable) if $IF(\xi_q, \tilde{f}_q, \tilde{\tau}_{q-1}^r, \tilde{\tau}_q^o, \tilde{\tau}_q^r)$ is guaranteed detectable.

Proof. Directly derived from Theorem 1. \square

Corollary 2. For the OWMA-TCC with $W \leq \tilde{W}^\#$ and a given significance level α , the q th IF is guaranteed detectable (G-detectable) if

$$\beta(\tilde{a}_{\tilde{W}^\#}^*)\tilde{f}_q^2 > 2\delta^2. \quad (52)$$

Then the window length W can be chosen such that $\tilde{W}^\# \geq W \geq \tilde{W}^*$, where

$$\tilde{W}^* = \arg \min_W \beta(\tilde{a}_W^*)\tilde{f}_q^2 > 2\delta^2. \quad (53)$$

Proof. Directly derived from Theorem 9 and Corollary 1. \square

Remark 8. A PF can be viewed as an IF with an infinite active duration. Thus, the developed methods as well as the above analyses, including all the theorems, propositions and corollaries, are applicable to PF by setting $\tau_{q-1}^r, \tau_q^o, \tau_q^r \rightarrow \infty$. Moreover, the developed OWMA method can be combined with dimensionality reduction techniques such as PCA and PLS to monitor specific subspaces, by replacing the measurement vector X with its score vector in corresponding subspaces.

5. Generalization to weakly stationary processes without the Gaussianity assumption

This section extends the above results to weakly stationary processes without the Gaussianity assumption. It can be seen from the previous sections that to implement the developed OWMA method, the autocovariance function R_l of the stationary process is needed, instead of the exact distribution of the stationary process. Thus, the developed OWMA method can be used in any stationary process with or without the Gaussianity assumption. Then, the remained question is to prove the optimality of the developed OWMA method in general stationary processes without Gaussianity assumption. Note that the stationary process here means the weakly stationary process, unless we specifically indicate otherwise.

It is worth pointing out that the T^2 statistic is widely adopted under both Gaussian and non-Gaussian conditions. It is well-known in the statistics [27] that under the condition of Gaussian distribution, the T^2 test is the uniformly most powerful unbiased test (UMPBT) of the hypothesis $H_0 : \mu_f = \mu$ versus $H_1 : \mu_f \neq \mu$. Therefore, the T^2 statistic has been widely accepted for hypothesis testing problem under the Gaussian condition. Later, due to its simple form and its optimal properties under the Gaussian condition, the T^2 statistic has been also widely adopted to detect anomalies under non-Gaussian conditions. In these cases, the T^2 statistic is understood as a measure of the process variation, and thus can be used in the process monitoring task under non-Gaussian conditions. Here, a little difference between the use of OWMA-TCC in stationary processes with and without the Gaussianity assumption is the calculation of the

control limit. Without the Gaussianity assumption, the WMA- T^2 statistic does not follow an F distribution, and thus the control limit can not be calculated by (7). Corresponding solutions are to use the empirical method [22] or the kernel density estimation (KDE) method [43] to calculate the control limit of $\tilde{T}_k^2(W)$, denoted as δ_w^2 , under non-Gaussian conditions.

Now we are in the position to show that, there is a sense in which the weight vector \tilde{a}_w^* defined by *Problem 1* and subsequently given in *Theorem 2* is also optimal for general weakly stationary processes. We consider that the stationary process is ergodic and N is sufficiently large. In this case, we have

$$\lim_{N \rightarrow \infty} \tilde{T}_k^2(W) = (\tilde{X}_k^f - \mu)^T \tilde{\Sigma}_W^{-1} (\tilde{X}_k^f - \mu), \quad (54)$$

and

$$\begin{aligned} \mathbb{E} \left\{ \lim_{N \rightarrow \infty} \tilde{T}_k^2(W) \right\} &= \mathbb{E} \left\{ \text{tr}[(\tilde{X}_k^f - \mu)(\tilde{X}_k^f - \mu)^T \tilde{\Sigma}_W^{-1}] \right\} \\ &= \text{tr} \left\{ \mathbb{E}[(\tilde{X}_k^f - \mu)(\tilde{X}_k^f - \mu)^T] \tilde{\Sigma}_W^{-1} \right\}, \end{aligned} \quad (55)$$

where \tilde{X}_k^f is modeled by (8), (9) and (11). Then, the mean of the WMA- T^2 statistic under the hypothesis of no fault, i.e., H_0 , is

$$\begin{aligned} \mathbb{E} \left\{ \lim_{N \rightarrow \infty} \tilde{T}_k^2(W) \middle| H_0 \right\} \\ = \text{tr} \left\{ \mathbb{E}[(\tilde{X}_k^* - \mu)(\tilde{X}_k^* - \mu)^T] \tilde{\Sigma}_W^{-1} \right\} = p, \end{aligned} \quad (56)$$

where the last equality is because the mean and covariance matrix of \tilde{X}_k^* are μ and $\tilde{\Sigma}_W$, respectively. In addition, the mean of the WMA- T^2 statistic under the hypothesis of IFs, i.e., H_1 , is

$$\begin{aligned} \mathbb{E} \left\{ \lim_{N \rightarrow \infty} \tilde{T}_k^2(W) \middle| H_1 \right\} \\ = \text{tr} \left\{ \mathbb{E}[(\tilde{X}_k^* - \mu + \xi_q f_q)(\tilde{X}_k^* - \mu + \xi_q f_q)^T] \tilde{\Sigma}_W^{-1} \right\} \\ = \text{tr} \left\{ [\tilde{\Sigma}_W + \xi_q \xi_q^T f_q^2] \tilde{\Sigma}_W^{-1} \right\} = \|\tilde{\Sigma}_W^{-1/2} \xi_q f_q\|^2 + p. \end{aligned} \quad (57)$$

By following (56) and (57), it can be seen that

$$\begin{aligned} \mathbb{E} \left\{ \lim_{N \rightarrow \infty} \tilde{T}_k^2(W) \middle| H_1 \right\} - \mathbb{E} \left\{ \lim_{N \rightarrow \infty} \tilde{T}_k^2(W) \middle| H_0 \right\} \\ = \|\tilde{\Sigma}_W^{-1/2} \xi_q f_q\|^2 = \lim_{N \rightarrow \infty} 2\beta(\tilde{a}_w) f_q^2, \end{aligned}$$

where $\beta(\tilde{a}_w)$ is the objective function of *Problem 1*.

For a hypothesis testing problem, one always prefers the distribution of the designed statistic to be as different as possible between two hypotheses. To this end, a widely used tool is the KL divergence. The KL divergence is designed to measure the difference between

two probability density functions (PDFs) [44]. However, calculation of the KL divergence needs exact PDFs of the distributions under two hypotheses. An alternative way is to measure the difference between two PDFs through the distance of their means, such as in [25]. Note that f_q is not a function of \tilde{a}_w . Therefore, $\beta(\tilde{a}_w)$ can measure the distribution difference of the WMA- T^2 statistic between two hypotheses in stationary processes. That is to say, the developed OWMA is optimal for weakly stationary processes in the sense of the statistic's distribution difference between two hypotheses.

Remark 9. *To sum up, the use of T^2 statistic is reasonable under both Gaussian and non-Gaussian conditions. Moreover, the developed OWMA-TCC is optimal for weakly stationary processes in the sense of the T^2 statistic's distribution difference between two hypotheses. To implement the developed OWMA method under non-Gaussian conditions, the only difference is to use the empirical method or the KDE method to calculate the control limit δ_w^2 . Note that the detectability analyses conducted in Section 3 do not employ the Gaussianity assumption. Hence, by replacing the control limit δ therein with δ_w , they become valid for weakly stationary processes. Properties of the OWMA method given in Section 4 are as well valid for weakly stationary processes.*

6. Simulation studies

In this section, two simulation examples are used to demonstrate the efficiency of the OWMA-TCC under both Gaussian and non-Gaussian conditions, by comparing with existing static and dynamic MSPM methods.

6.1. A numerical example

A multivariate AR(1) process model used in the original DPCA literature [45] is employed here to illustrate the effectiveness and efficiency of the developed method, in comparison with several well-known methods. The process model under normal operating conditions is

$$\begin{aligned} \mathbf{z}_k &= \begin{bmatrix} 0.118 & -0.191 \\ 0.847 & 0.264 \end{bmatrix} \mathbf{z}_{k-1} + \begin{bmatrix} 1 & 2 \\ 3 & -4 \end{bmatrix} \mathbf{u}_{k-1}, \\ \mathbf{y}_k &= \mathbf{z}_k + \mathbf{v}_k, \end{aligned} \quad (58)$$

where \mathbf{u} is the correlated input:

$$\mathbf{u}_k = \begin{bmatrix} 0.811 & -0.226 \\ 0.477 & 0.415 \end{bmatrix} \mathbf{u}_{k-1} + \begin{bmatrix} 0.193 & 0.689 \\ -0.320 & -0.749 \end{bmatrix} \mathbf{w}_{k-1}.$$

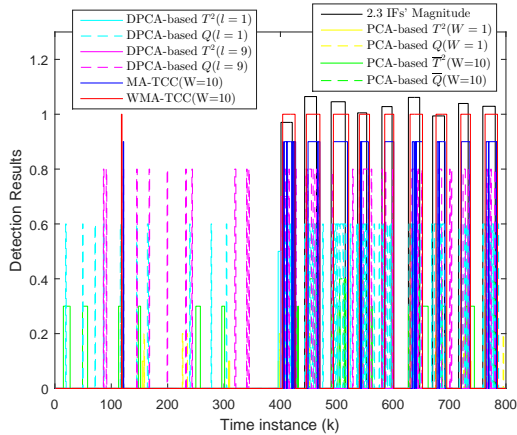


Figure 2: IFD results using different methods in the numerical simulation (Gaussian noise).

According to [45], the noises \mathbf{w} and \mathbf{v} are zero means, and follow Gaussian distributions with variance 1 and 0.1, respectively. Both \mathbf{u} and \mathbf{y} are measured so that we can form the process data as $X_k = [\mathbf{y}_k; \mathbf{u}_k]$.

Both 5000 sets of 10 consecutive observations (training samples) and 800 consecutive observations (test samples) are generated according to (58), and intermittent process faults are subsequently introduced in the test dataset since sample 401. The first 400 test samples are used to calculate false alarm rates (FARs) of different methods. The introduced IFs have an additive form as modeled by (11) with the fault direction $\xi_q = [0.0319, -0.2740, 0.9611, -0.0098]^T$, the lower bound of each fault magnitude $\tilde{f}_q = 0.42$, the lower bound of each fault active and inactive duration $\tilde{\tau}_q^o = 15$, $\tilde{\tau}_q^r = 20$. The actual fault magnitude, fault active and inactive duration are all generated randomly according to their lower bounds and are shown in Fig. 2 with a black line (the Y-axis shows the fault magnitude multiplied by 2.3, and the X-axis shows the fault active and inactive duration).

Training samples are used to determine the optimal weight vector and the significance level α is set as 0.01. Then, we can conclude that the introduced IFs are guaranteed detectable by the OWMA-TCC with window length $W \in [10, 15]$, according to *Theorems 1* and 9 and *Corollary 2*. The OWMA-TCC with window length $W = 10$ is given in Fig. 3 with a red line. To demonstrate the importance of employing an optimal weight vector, the WMA-TCC with the equally weighted scheme, denoted here as MA-TCC, with window length $W = 10$ is also given in Fig. 3 for comparison. It is noted that the MA-TCC fluctuates around its control limit

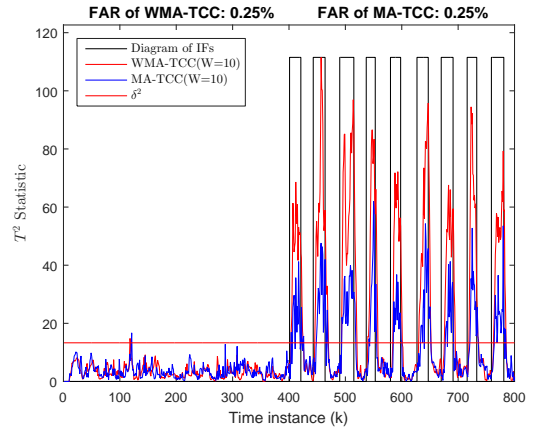


Figure 3: IFD using the OWMA-TCC and MA-TCC with window length $W = 10$ in the numerical simulation (Gaussian noise).

whereas the OWMA-TCC goes beyond its control limit clearly. This phenomenon can be explained by *Theorem 1*, which says that the introduced IFs are not guaranteed detectable by the MA-TCC(10). Overall, their detailed IFD results are given in Fig. 2 with blue and red lines, respectively.

Several static and dynamic MSPM methods are used here to show their limitations on dealing with IFs. Another 50000 consecutive observations are generated according to (58) as training samples for these MSPM methods. The traditional PCA and its MA-based extension (i.e., the MA-PCA [26]), are selected as the representatives of static MSPM methods. For PCA and MA-PCA models, the cumulative percent variance (CPV) criterion says that three PCs should be chosen, which account for more than 95% of the variance in original variables. The MA-PCA-based T^2 and Q statistics with window length $W = 10$, denoted here as PCA-based $\bar{T}^2(10)$ and PCA-based $\bar{Q}(10)$, are utilized for comparison. The PCA-based and MA-PCA-based control charts of the test data are given in Fig. 4. Moreover, their detailed IFD results are given in Fig. 2 with yellow and green lines, respectively. It can be seen that traditional PCA is inefficient for IFs and the MA-PCA has an unacceptable high FAR (11%). This high FAR is expected since several studies [24, 45, 46] have already indicated that monitoring autocorrelated data using static MSPM methods tends to produce excessive false alarms.

As for dynamic MSPM methods, we select DPCA [45] as their representative in this subsection, because the simulation model (58) was first introduced therein. According to [45], the time lag is determined as $l = 1$, and five PCs are chosen for the DPCA model. The

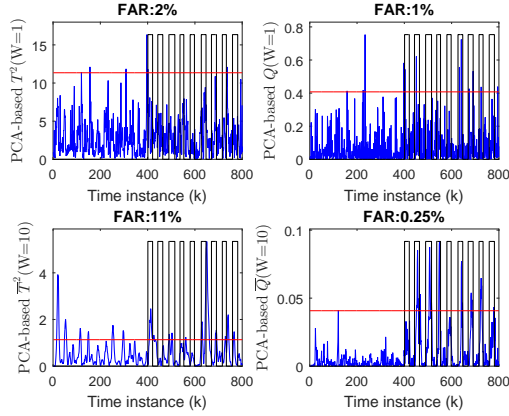


Figure 4: IFD using PCA-based and MA-PCA-based ($W = 10$) control charts in the numerical simulation (Gaussian noise).

DPCA-based T^2 and Q statistics of the test data are given in Fig. 5. Moreover, their detailed IFD results are given in Fig. 2 with solid and dashed cyan lines, respectively. It is obvious that the IFD performance of both statistics is far from satisfactory. For further comparison, the time lag is chosen as $l=9$, so that the same number of samples with OWMA-TCC(10), i.e., 10 samples, can be utilized to detect IFs at each time instance. According to the CPV criterion, twelve PCs should be chosen for the DPCA model at this time, which account for more than 99% of the variance in original variables. The DPCA-based $T^2(l=9)$ and $Q(l=9)$ statistics of the test data are given in Fig. 5, along with their detailed IFD results given in Fig. 2 with solid and dashed magenta lines, respectively. It can be seen that the IFD performance is still unsatisfactory.

To demonstrate the effectiveness of the developed method under non-Gaussian conditions, the noises \mathbf{w} and \mathbf{v} are reset to uniform distributions $\mathbb{U}(-0.5, 0.5)$ and $\sqrt{0.1}\mathbb{U}(-0.5, 0.5)$, respectively. Except for this and resetting the lower bound of each fault magnitude to $\tilde{f}_q = 0.105$, other parameters of the numerical example remain unchanged. A present MSPM method used for IFD under Gaussian or non-Gaussian condition, i.e., the MW-KD [21], is employed. According to [21], three PCs which account for more than 95% of the original variance should be retained, and the threshold is set accordingly. The empirical method [22] is used here to set the control limits of OWMA-TCC and MA-TCC. The statistics of OWMA-TCC(10), MA-TCC(10) and MW-KD(10) are given in Fig. 6. Their detailed IFD results are given in Fig. 7 with red, blue and dashed black lines, respectively. Moreover, IFD results of the above-

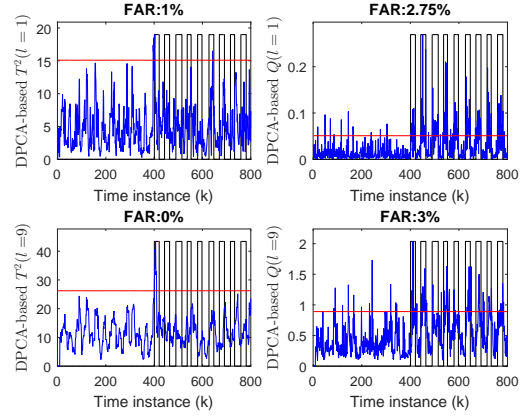


Figure 5: IFD using DPCA-based control charts with time lag $l = 1$ and $l = 9$ in the numerical simulation (Gaussian noise).

mentioned static and dynamic MSPM methods are also given therein. By comparison, the importance of employing an optimal weight vector is observed.

To appreciate the performance of different methods, their IFD results under Gaussian and non-Gaussian conditions are shown together in Figs. 2 and 7, respectively. It is noted that only OWMA-TCC goes beyond its control limit clearly when an IF occurs, under both Gaussian and non-Gaussian conditions. By contrast, the others tend to fluctuate around their corresponding control limits. Thus, it can be seen that the developed method shows better IFD performance among several static and dynamic MSPM methods.

6.2. The CSTR process

In this subsection, a continuous stirred tank reactor (CSTR) simulation is utilized to demonstrate the effectiveness and efficiency of the proposed methods through comparative studies. The CSTR process can be described by the following differential equations

$$\begin{aligned} \frac{dC_A}{dt} &= \frac{q}{V}(C_{Af} - C_A) - k_0 \exp\left(-\frac{E}{RT}\right)C_A + v_1, \\ \frac{dT}{dt} &= \frac{q}{V}(T_f - T) - \frac{\Delta H}{\rho C_p}k_0 \exp\left(-\frac{E}{RT}\right)C_A + \frac{UA}{V\rho C_p}(T_c - T) + v_2, \end{aligned} \quad (59)$$

where $C_A, T, T_c, q, C_{Af}, T_f$ are the outlet concentration, reactor temperature, cooling water temperature, feed flow rate, feed concentration and feed temperature, respectively. v_1 and v_2 are independent Gaussian white noises. The measured variables are $[C_A, T, T_c, q]^T$, where $[C_A, T]^T$ are controlled variables with nominal values, and $[T_c, q]^T$ are manipulated variables with feedback control. More detailed descriptions of the CSTR

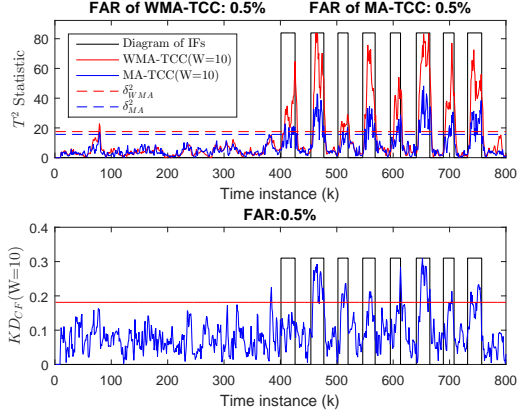


Figure 6: IFD using the OWMA-TCC, MA-TCC and MW-KD with window length $W = 10$ in the numerical simulation (uniformly distributed noise).

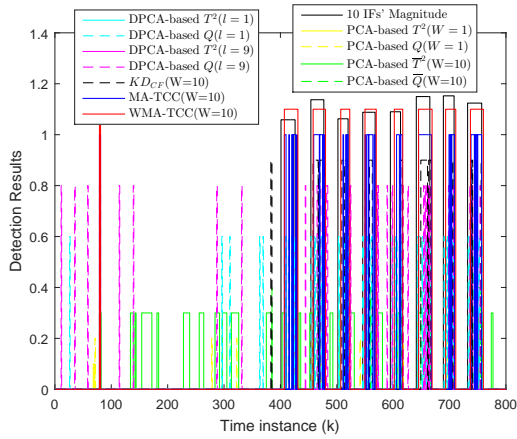


Figure 7: IFD results using different methods in the numerical simulation (uniformly distributed noise).

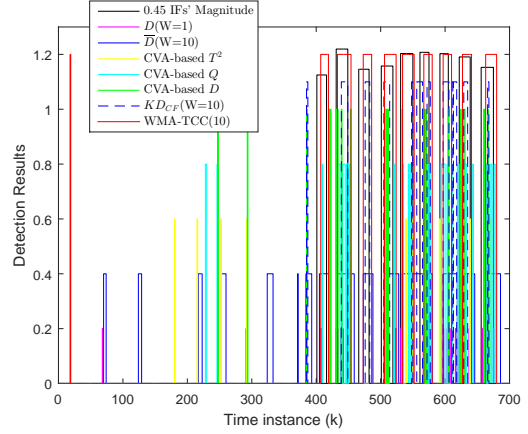


Figure 8: IFD results using different methods in the CSTR process (Gaussian noise).

process can be found in [47], where the settings of the process, including system parameters and conditions as well as controller information, are also given therein. Different from most existing literature that always sets the sampling interval as 1min (in this situation, process data are nearly independent), we choose the sampling interval as 3s here because of the higher sampling frequency requirement for capturing IFs. Note that shortening the sampling interval results in autocorrelated process data.

The unmeasurable feed temperature T_f is a main disturbance in the process, and has been used by many studies [48, 49] to evaluate different FD methods. In this simulation, intermittent increases of feed temperature T_f are introduced since sample 401, with a lower bound of each fault magnitude $\tilde{f}_q = 2.5\text{K}$, a lower bound of each fault active, and inactive duration $\tilde{\tau}_q^o = \tilde{\tau}_q^r = 10$ sampling intervals, i.e., 30s. The first 400 samples are used to calculate FARs of different methods. A total of 700 consecutive observations are collected as test samples. The actual fault magnitude, fault active and inactive duration are all generated randomly according to their lower bounds and are shown in Fig. 8 with a black line (the Y-axis shows the fault magnitude multiplied by 0.45, and the X-axis shows the fault active and inactive duration).

According to the process model (59), T_f directly affects the reactor temperature T . However, since T is controlled by manipulating the cooling water temperature T_c , when T deviates from its nominal value, T_c is immediately adjusted to compensate the change. In this way, the entire process is always under control, rendering the system parameters and conditions un-

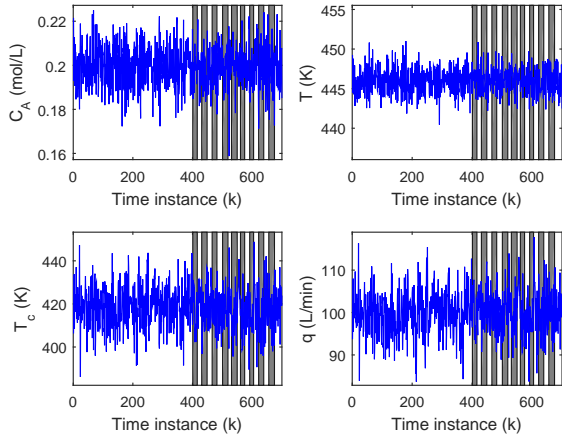


Figure 9: Measured CSTR process variables with intermittent disturbances in the feed temperature T_f (Gaussian noise).

changed. Therefore, when intermittent disturbances of T_f occur, C_A , T , q are still around their set-point values, whereas T_c exhibits intermittent biases instead. This phenomenon is also shown in Fig. 9, where collected process data with intermittent disturbances in T_f are plotted and the gray shadows represent the active duration of IFs. Moreover, note that the correlations (autocorrelation and cross-correlation) of process variables in this scenario remain unchanged. This can be seen from (59) that time constants of C_A , T are irrelevant with T_f , T_c . As a result, the introduced intermittent disturbances in T_f can be well modeled by (11) with fault direction $\xi_q = [0, 0, 1, 0]^T$.

Five thousand sets of 10 consecutive observations are collected under normal conditions as training samples, which are subsequently utilized to determine the optimal weight vector and the control limit with significance level $\alpha = 0.01$. Then, we can conclude that the introduced intermittent disturbances in T_f are guaranteed detectable by the OWMA-TCC with window length $W = 10$, according to *Theorems 1* and *9* and *Corollary 2*. Several well-known static and dynamic MSPM methods are also employed here for comparison. The Mahalanobis distance (MD) (also known as the global Hotelling's T^2 test D) [2], and its MA-based extension [26] with window length $W = 10$, i.e., $\bar{D}(10)$, are chosen as representatives of static MSPM methods. As for dynamic MSPM methods, CVA is chosen as their representative. Additionally, the MW-KD is also chosen. Another 50,000 consecutive observations are collected under normal conditions as training samples for these

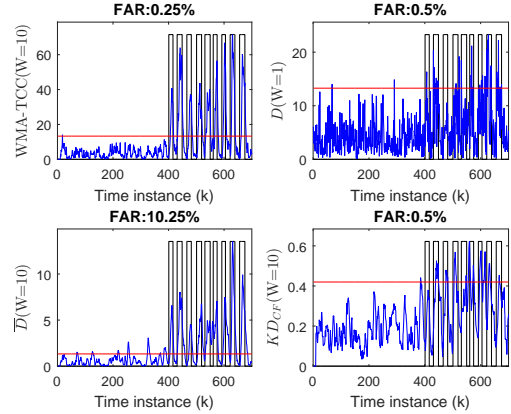


Figure 10: IFD using OWMA-TCC, MD, MA-MD and MW-KD in the CSTR process (Gaussian noise).

MSPM methods.

The OWMA-TCC(10), $D(1)$, $\bar{D}(10)$ and $KD_{CF}(10)$ control charts of the test data are given in Fig. 10. Moreover, their detailed IFD results are given in Fig. 8 with red, magenta, blue and dashed blue lines, respectively. For $KD_{CF}(10)$, two PCs which account for more than 95% of the original variance are retained [21]. It can be seen that the $D(1)$ statistic is inefficient for IFs. While the traditional MA technique can indeed improve the statistics' sensitivity to IFs, it causes an unacceptable high FAR (10.25%) when process data are autocorrelated, and consequently invalidates the online monitoring approach. By contrast, the proposed OWMA-TCC goes beyond its control limit clearly when IFs occur, and the FAR is consistent with its theoretical value, i.e., less than 1%. As for the CVA model, according to [43], the number of time lags for past (p) and future (f) observations is determined using autocorrelation analysis on the training samples. For the simulation, it has been found that three time lags are the maximum, after which autocorrelations become insignificant for the summed squares of all measurements as well as for all the process variables, at 99% confidence level. Thus, we set $p = f = 3$. In addition, the number of states is chosen as four according to the dominant singular value (SV) method (to find the point where a "knee" appears in the SV curve). The CVA-based T^2 , Q , D statistics [43] of the test data are given in Fig. 11, and their detailed IFD results are given in Fig. 8 with yellow, cyan and green lines, respectively. The IFD results indicate that CVA also has limitations on dealing with IFs. The time lags of CVA are chosen only based on system dynamics without taking the characteristics of IFs into account,

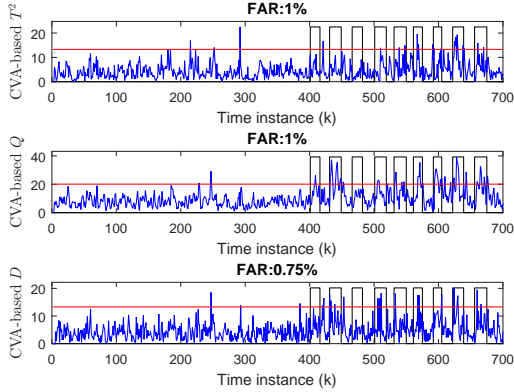


Figure 11: IFD using CVA-based control charts in the CSTR process (Gaussian noise).

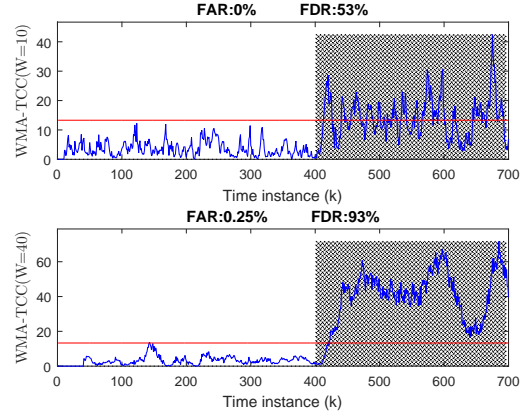


Figure 12: IFD using OWMA-TCC in the CSTR process ($\tau_q^o = \tau_q^r = 1$, Gaussian noise).

resulting in a lack of sensitivity to IFs of the method.

In the case of $\tau_q^o = \tau_q^r = 1$, the statistics of OWMA-TCC(10) and OWMA-TCC(40) are given in Fig. 12. It can be seen that due to the violation of $W \leq W^\#$, although the control chart still alarms, we can not determine each appearance (disappearance) of an IF before its subsequent disappearance (appearance). Moreover, due to the inclusion of both faulty and fault-free samples in the time window, the detectability condition is no more satisfied when $W = 10$, resulting in the missed alarms. Nevertheless, the developed OWMA-TCC is still applicable in this case due to the efforts we have made in improving the existing MA-type schemes to smooth autocorrelated data. By enlarging the window length W from 10 to 40, the missed alarms can be totally eliminated after some delay. In addition, to demonstrate the effectiveness of the developed method under non-Gaussian conditions, the noises v_1 and v_2 are reset to the uniform distribution $0.1U(-0.5, 0.5)$. Except for this and resetting the lower bound of each fault magnitude to $\tilde{f}_q = 1.2$, other parameters of the simulated CSTR process remain unchanged. IFD results of the above-mentioned MSPM methods are given in Fig. 13. By comparison, the better IFD performance of the OWMA-TCC is observed.

Finally, to appreciate the performance of different methods, their IFD results under Gaussian and non-Gaussian conditions are shown together in Figs. 8 and 13, respectively. It is noted that OWMA-TCC alarms continuously when an IF occurs. By contrast, the others tend to alarm sporadically, or start to alarm after the IF has disappeared. Overall, it can be seen that the developed method shows better IFD performance among the

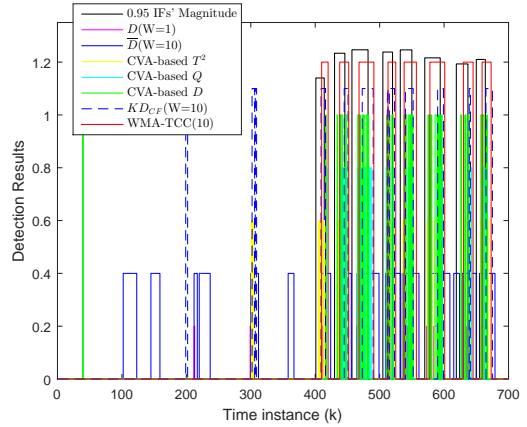


Figure 13: IFD results using different methods in the CSTR simulation (uniformly distributed noise).

static and dynamic MSPM methods being compared.

7. Conclusion and future perspective

In this paper, a weighted moving average (WMA) scheme has been combined with the Hotelling's T^2 statistic to form an optimally weighted MA (OWMA) T^2 control chart (OWMA-TCC) used in weakly stationary processes. Compared with static MSPM methods such as PCA, OWMA-TCC employs a time window and an optimal weight vector (OWV) to improve its detection capability for IFs that always manifest themselves as repeated small and short fluctuations. Compared with traditional MA-type schemes such as MA-PCA, OWMA-TCC overcomes the problem of produc-

ing excessive false alarms when data exhibit autocorrelation, because it does not assume data to be independent. Moreover, OWMA-TCC can use the correlation (autocorrelation and cross-correlation) information to increase its sensitivity to IFs by finding an OWV. Compared with dynamic MSPM methods such as DPCA and CVA, OWMA-TCC selects the window length considering the characteristics of IFs, i.e., the fault duration and magnitude, and then gains additional sensitivity to IFs by optimizing its weights.

The non-optimality of the equally and exponentially weighted scheme used for fault detection when data have autocorrelation has been discovered. The essence that existing MA-type schemes do not effectively utilize the correlation information of samples has been revealed. Then, an OWMA theory has been established, including methods to construct WMA statistics, analyze the fault detectability, and determine the OWV. Existence of the OWV has been proven with the help of the Brouwer fixed-point theory, and an iteration process to obtain the OWV has been provided. These ensure that the OWMA-TCC is implementable in real applications. Moreover, we have found that the OWV possesses a symmetry structure, and the equally weighted scheme is optimal for any IF directions when data exhibit no autocorrelation. This verifies the optimality of existing MA-based MSPM methods when applied to independent data. The developed method has been evaluated using a numerical example and the CSTR process. Simulation results have shown that for IFs with same direction, magnitude and duration, the compared methods, including several well-known static and dynamic MSPM methods, fail to detect them whereas OWMA-TCC succeeds in detecting them.

Further studies include the combination of OWMA with recursive methods, other statistics, kernel methods, dynamic data modeling methods and other selection criteria, to address the problems of monitoring processes with slightly varying operation points, varying levels of noise, nonlinear properties and nonstationary properties, as well as detecting faults with unknown characteristics.

References

- [1] M. S. Choudhury, S. L. Shah, and N. F. Thornhill. Diagnosis of poor control-loop performance using higher-order statistics. *Automatica*, 40:1719–1728, 2004.
- [2] S. J. Qin. Statistical process monitoring: basics and beyond. *Journal of Chemometrics*, 17(8–9):480–502, 2003.
- [3] U. Kruger, Y. Q. Zhou, and G. W. Irwin. Improved principal component monitoring of large-scale processes. *Journal of Process Control*, 14(8):879–888, 2004.
- [4] S. J. Wierda. Multivariate statistical process control—recent results and directions for future research. *Statistica Neerlandica*, 48(2):147–168, 1994.
- [5] D. H. Zhou, Y. H. Zhao, Z. D. Wang, X. He, and M. Gao. Review on diagnosis techniques for intermittent faults in dynamic systems. *IEEE Transactions on Industrial Electronics*, 67(3):2337–2347, 2020.
- [6] L. K. Carvalho, M. V. Moreira, and J. C. Basilio. Diagnosability of intermittent sensor faults in discrete event systems. *Automatica*, 79:315–325, 2017.
- [7] J. F. Zhang, P. D. Christofides, X. He, Z. Wu, Y. H. Zhao, and D. H. Zhou. Robust detection of intermittent sensor faults in stochastic ltv systems. *Neurocomputing*, 388:181–187, 2020.
- [8] N. H. Obeid, A. Battiston, T. Boileau, and B. Nahid-Mobarakeh. Early intermittent interturn fault detection and localization for a permanent magnet synchronous motor of electrical vehicles using wavelet transform. *IEEE Transactions on Transportation Electrification*, 3(3):694–702, 2017.
- [9] S. Singh, H. S. Subramania, S. W. Holland, and J. T. Davis. Decision forest for root cause analysis of intermittent faults. *IEEE Transactions on Systems, Man, and Cybernetics, Part C: Applications and Reviews*, 42(6):1818–1827, 2012.
- [10] B. P. Cai, Y. Liu, and M. Xie. A dynamic-bayesian-network-based fault diagnosis methodology considering transient and intermittent faults. *IEEE Transactions on Automation Science and Engineering*, 14(1):276–285, 2017.
- [11] D. N. Monekosso and P. Remagnino. Data reconciliation in a smart home sensor network. *Expert Systems with Applications*, 40(8):3248–3255, 2013.
- [12] Y. C. Du, H. Budman, and T. A. Duever. Comparison of stochastic fault detection and classification algorithms for nonlinear chemical processes. *Computers and Chemical Engineering*, 106:57–70, 2017.
- [13] Y. C. Du, H. Budman, T. A. Duever, and D. P. Du. Fault detection and classification for nonlinear chemical processes using lasso and gaussian process. *Industrial & Engineering Chemistry Research*, 57(27):8962–8977, 2018.
- [14] G. Niu, L. J. Xiong, X. X. Qin, and M. Pecht. Fault detection isolation and diagnosis of multi-axle speed sensors for high-speed trains. *Mechanical Systems and Signal Processing*, 131:183–198, 2019.
- [15] Y. H. Zhao, X. He, and D. H. Zhou. Intermittent fault detection with T^2 control chart. *IFAC-PapersOnLine*, 51(24):1298–1304, 2018.
- [16] Y. H. Zhao, X. He, and D. H. Zhou. Detecting intermittent faults with moving average techniques. In *2019 IEEE 15th International Conference on Automation Science and Engineering*, pages 1712–1717. IEEE, 2019.
- [17] L. L. Li, Z. H. Wang, and S. Yi. Fault diagnosis for the intermittent fault in gyroscopes: A data-driven method. In *35th Chinese Control Conference (CCC)*, pages 6639–6643, 2016.
- [18] A. Bakdi and A. Kouadri. A new adaptive PCA based thresholding scheme for fault detection in complex systems. *Chemometrics & Intelligent Laboratory Systems*, 162:83–93, 2017.
- [19] A. Bakdi, A. Kouadri, and A. Bensmail. Fault detection and diagnosis in a cement rotary kiln using PCA with EWMA-based adaptive threshold monitoring scheme. *Control Engineering Practice*, 66:64–75, 2017.
- [20] A. Bakdi, W. Bounoua, S. Mekhilef, and L. M. Halabi. Nonparametric Kullback-divergence-PCA for intelligent mismatch detection and power quality monitoring in grid-connected rooftop PV. *Energy*, 189:116366, 2019.
- [21] S. Kammammettu and Z. K. Li. Change point and fault detection using kantorovich distance. *Journal of Process Control*, 80:41–59, 2019.

- [22] J. Shang, M. Y. Chen, H. Q. Ji, and D. H. Zhou. Recursive transformed component statistical analysis for incipient fault detection. *Automatica*, 80:313–327, 2017.
- [23] Wang Lin, Chun Jie Yang, and Youxian Sun. Multimode process monitoring approach based on moving window hidden markov model. *Industrial & Engineering Chemistry Research*, 57(1):292–301, 2018.
- [24] U. Kruger, S. Kumar, and T. Littler. Improved principal component monitoring using the local approach. *Automatica*, 43:1532–1542, 2007.
- [25] J. H. Chen, C. M. Liao, F. R. J. Lin, and M. J. Lu. Principle component analysis based control charts with memory effect for process monitoring. *Industrial & Engineering Chemistry Research*, 40(6):1516–1527, 2001.
- [26] H. Q. Ji, X. He, J. Shang, and D. H. Zhou. Incipient fault detection with smoothing techniques in statistical process monitoring. *Control Engineering Practice*, 62:11–21, 2017.
- [27] T. W. Anderson. *An Introduction to Multivariate Statistical Analysis (3rd edition)*. Wiley-Interscience, Hoboken, NJ, 2003.
- [28] H. Q. Ji, X. He, J. Shang, and D. H. Zhou. Incipient sensor fault diagnosis using moving window reconstruction-based contribution. *Industrial & Engineering Chemistry Research*, 55(10):2746–2759, 2016.
- [29] H. T. Chen, B. Jiang, N. Y. Lu, and Z. H. Mao. Deep PCA based real-time incipient fault detection and diagnosis methodology for electrical drive in high-speed trains. *IEEE Transactions on Vehicular Technology*, 67(6):4819–4830, 2018.
- [30] C. F. Alcalá and S. J. Qin. Reconstruction-based contribution for process monitoring. *Automatica*, 45(7):1593–1600, 2009.
- [31] C. Shang, F. Yang, B. Huang, and D. X. Huang. Recursive slow feature analysis for adaptive monitoring of industrial processes. *IEEE Transactions on Industrial Electronics*, 65(11):8895–8905, 2018.
- [32] H. T. Chen, B. Jiang, W. Chen, and H. Yi. Data-driven detection and diagnosis of incipient faults in electrical drives of high-speed trains. *IEEE Transactions on Industrial Electronics*, 66(6):4716–4725, 2019.
- [33] B. Mnassri, E. M. E. Adel, and M. Ouladsine. Generalization and analysis of sufficient conditions for pca-based fault detectability and isolability. *Annual Reviews in Control*, 37(1):154–162, 2013.
- [34] R. Isermann. Model-based fault-detection and diagnosis – status and applications. *Annual Reviews in control*, 29(1):71–85, 2005.
- [35] J. F. Zhang, P. D. Christofides, X. He, F. Albalawi, Y. H. Zhao, and D. H. Zhou. Intermittent sensor fault detection for stochastic ltv systems with parameter uncertainty and limited resolution. *International Journal of Control*, 93(4):788–796, 2020.
- [36] R. Dunia and S. J. Qin. A unified geometric approach to process and sensor fault identification and reconstruction: the unidimensional fault case. *Computers and Chemical Engineering*, 22(7–8):927–943, 1998.
- [37] R. Dunia and S. J. Qin. Subspace approach to multidimensional fault identification and reconstruction. *Aiche Journal*, 44(8):1813–1831, 1998.
- [38] S. Biswas. Diagnosability of discrete event systems for temporary failures. *Computers & Electrical Engineering*, 38(6):1534–1549, 2012.
- [39] J. F. Zhang, P. D. Christofides, X. He, Y. H. Zhao, Z. H. Zhang, and D. H. Zhou. Robust detection of intermittent multiplicative sensor fault. *Asian Journal of Control*, Published online, DOI: 10.1002/asjc.2241.
- [40] D. G. Luenberger and Y. Ye. *Linear and nonlinear programming (3rd edition)*. Springer Science, New York, NY, 2008.
- [41] A. C. Chiang and K. Wainwright. *Fundamental methods of mathematical economics (4th edition)*. McGraw-Hill/Irwin, New York, NY, 2005.
- [42] E. Zeidler. *Nonlinear Functional Analysis and Its Applications I: Fixed-Point Theorems (1st edition)*. Springer-Verlag, New York, NY, 1986.
- [43] K. E. S. Pilario and Y. Cao. Canonical variate dissimilarity analysis for process incipient fault detection. *IEEE Transactions on Industrial Informatics*, 14(12):5308–5315, 2018.
- [44] J. S. Zeng, U. Kruger, J. Geluk, X. Wang, and L. Xie. Detecting abnormal situations using the kullback–leibler divergence. *Automatica*, 50(11):2777–2786, 2014.
- [45] W. F. Ku, R. H. Storer, and C. Georgakis. Disturbance detection and isolation by dynamic principal component analysis. *Chemometrics and Intelligent Laboratory Systems*, 30(1):179–196, 1995.
- [46] C. Guo, W. K. Hu, S. Q. Lai, F. Yang, and T. W. Chen. An accelerated alignment method for analyzing time sequences of industrial alarm floods. *Journal of Process Control*, 57:102–115, 2017.
- [47] G. Li, S. J. Qin, Y. D. Ji, and D. H. Zhou. Reconstruction based fault prognosis for continuous processes. *Control Engineering Practice*, 18(10):1211–1219, 2010.
- [48] J. Shang, M. Y. Chen, H. Q. Ji, D. H. Zhou, and M. L. Li. Dominant trend based logistic regression for fault diagnosis in nonstationary processes. *Control Engineering Practice*, 66:156–168, 2017.
- [49] C. Shang, F. Yang, X. Q. Gao, X. L. Huang, J. A. K. Suykens, and D. X. Huang. Concurrent monitoring of operating condition deviations and process dynamics anomalies with slow feature analysis. *AICHE Journal*, 61(11):3666–3682, 2015.